

# Phase encoding a reflector array using open and short-circuited loads



**Prepared by:**  
Benco Loots

**Prepared for:**  
Dr Stephen Paine  
Department of Electrical Engineering  
University of Cape Town

Submitted to the Department of Electrical Engineering at the University of Cape Town  
in partial fulfilment of the academic requirements for a  
MEng Master of Engineering Specialising in Radar

# Declaration

1. I know that plagiarism is wrong. Plagiarism is to use another's work and pretend that it is one's own.
2. I have used the IEEE convention for citation and referencing. Each contribution to, and quotation in, this report from the work(s) of other people has been attributed, and has been cited and referenced.
3. This report is my own work.
4. I have not allowed, and will not allow, anyone to copy my work with the intention of passing it off as their own work or part thereof.



July 31, 2025

---

NAME SURNAME

Date

# Acknowledgements

I would like to sincerely thank my supervisors, Dr. Stephen Paine and Dr. Gideon Wiid for the support during my research. Many thanks to the former Reutech CTO Pieter-Jan Wolfaardt for the support as well as the wonderful research topic.

I am grateful to my mother, Sunette, for the sacrifices made to allow me to complete my degree.

Thank you to everyone at Reutech, Fayruz Crombie, Shaba, Jurgens de Jager and Mike Movious for the vacation work opportunities to improve my skills and get involved in the world of radars.

# Abstract

Designing an Electronically Steered Array (ESA) requires a feed network. Four main types of feed networks are used namely Series, Parallel, Space-Fed and Reflective Space-Fed. All these feed networks require a phase shifter for each of antenna elements. Since ESA's commonly consists of more than 1000 antenna elements each requiring its own expensive phase shifter. Therefor designing a low-cost ESA is nearly impossible, especially at high frequencies. To address this, a system is proposed that does not steer the phase in small increments but rather encodes an array's elements with a fixed phase by switching the antenna load from an open to a short circuit and back. This report details the first necessary investigation to prove the feasibility of this system. For this proposed system one must verify that it is possible to induce a fixed phase difference on a reflector antenna by merely changing the load from open to short. Only if this possible will can the system be designed further.

For this investigation a X-band antenna is designed with the focus on being able to change the load between short, open and matched load. Using the Rohde & Schwarz ZVA40 VNA and two X-Band Horn antennas, the designed antennas are tested for all loads. The measurements are processed further in MATLAB to isolate the phase change due to the antenna load and verify that it is possible to not only encode but also extract a fixed phase difference on the reflector array elements.

# Contents

<b>List of Figures</b>	<b>vii</b>
<b>List of Tables</b>	<b>x</b>
<b>1 Introduction</b>	<b>1</b>
1.1 Background . . . . .	1
1.2 Problem Statement . . . . .	1
1.3 Objectives . . . . .	1
1.4 System Requirements . . . . .	2
1.5 Scope & Limitations . . . . .	2
1.6 Report Outline . . . . .	2
<b>2 Literature Review</b>	<b>3</b>
2.1 Antenna . . . . .	3
2.1.1 Antenna Gain . . . . .	3
2.1.2 Nearfield & Farfield . . . . .	3
2.1.3 Monopole Antenna . . . . .	4
2.1.4 Patch Antenna . . . . .	4
2.1.5 Horn Antenna . . . . .	5
2.2 Radar Range Equation . . . . .	6
2.3 Frequency bands . . . . .	6
2.4 RF system impedance ( $50 \Omega$ matched systems) . . . . .	7
2.4.1 Smith Chart . . . . .	7
2.5 Dielectric materials . . . . .	8
2.5.1 PCB Transmission lines . . . . .	8
2.5.2 Coaxial Cables . . . . .	9
2.6 FMCW . . . . .	9
2.7 RF simulation software . . . . .	9
2.7.1 FEKO . . . . .	10
2.7.2 CST . . . . .	10
2.8 ESA . . . . .	12
2.8.1 ESA Feeds . . . . .	12
2.9 Permittivity and Permeability . . . . .	12
2.10 VNA . . . . .	13
<b>3 System Design</b>	<b>14</b>
3.1 Simulation based investigation . . . . .	14

3.1.1	Antenna design and ports in FEKO . . . . .	15
3.1.2	Phase & Planar wave & Dipole monitor . . . . .	17
3.1.3	Coax & CPW . . . . .	18
3.1.4	CST Studio . . . . .	21
3.2	Antenna Detail Design . . . . .	22
3.2.1	Center frequency . . . . .	22
3.2.2	PCB Stack-up . . . . .	22
3.2.3	Patch Dimensions . . . . .	23
3.2.4	Feed inset . . . . .	27
3.2.5	Masking the changing of the feed . . . . .	28
3.2.6	Masking the changing of the feed . . . . .	30
3.2.7	Linear & 2D reflector array design . . . . .	31
3.2.8	Manufacturing . . . . .	35
3.3	Measurement Processing . . . . .	38
<b>4</b>	<b>Testing &amp; Results</b>	<b>41</b>
4.1	Test setup & Equipment . . . . .	41
4.2	Results . . . . .	43
<b>5</b>	<b>Conclusions</b>	<b>51</b>
<b>Bibliography</b>		<b>52</b>
<b>A Repository Locations</b>		<b>54</b>

# List of Figures

2.1	A typical Antenna pattern.	3
2.2	Transition from spherical waves to planar waves.	4
2.3	Monopole model and 3D antenna pattern.	4
2.4	Patch antenna model and antenna pattern.	5
2.5	Fringing fields on a patch antenna.	5
2.6	A typical horn antenna.	6
2.7	Assigned Frequency Band in the EM spectrum.	6
2.8	Reflection of a sinusoidal wave at an open circuit (left) and short circuit (right).	7
2.9	Smith chart and how lumped element move on the smith chart.	7
2.10	Microstrip model.	8
2.11	Stripline model (left), CPW model (middle) and GCPW model (right).	8
2.12	Coaxial Cable.	9
2.13	Pulsed waveform (left), FMCW waveform (right).	9
2.14	Running a parameter sweep in FEKO.	10
2.15	Available ports and sources in FEKO.	10
2.16	Available ports and sources in CST.	11
2.17	Port extension coefficient macro in CST.	11
2.18	Parameter sweep in CST.	11
2.19	Angle extraction setup.	12
2.20	Four types of ESA feeds.	12
2.21	Scattering parameters diagram.	13
3.1	Wave incident at a dielectric boundary.	14
3.2	Patch antenna model in FEKO using a wire port.	15
3.3	Return loss of the patch in figure 3.2	15
3.4	Antenna pattern of the patch in figure 3.2	16
3.5	Patch antenna model in FEKO using a edge port.	16
3.6	Return loss of the patch in figure 3.5	16
3.7	FEKO simulation setup using a dipole with a wire port as the monitor.	17
3.8	Visual representation of the unbounded planar wave source in FEKO.	17
3.9	FEKO simulation setup using a farfield monitor.	18
3.10	Patch antenna model with a variable coaxial cable	18
3.11	Microstrip model in FEKO using a edge port along with the frequency response.	19
3.12	CPW model in FEKO using a edge port along with the frequency response.	19
3.13	CPW model in FEKO using the supplied port from Altair support.	20
3.14	Frequency response of the CPW model in figure 3.13	20
3.15	X-band frequency response of the CPW model in figure 3.13	20

3.16 CPW model in CST using waveguide ports.	21
3.17 Meshed CPW model in CST.	21
3.18 X-band frequency response of the CPW model in figure 3.16	21
3.19 Line impedance of the CPW model in figure 3.16.	22
3.20 PCB stackup used for the antenna design.	23
3.21 Roger Corporation's Microwave Impedance Calculator.	23
3.22 Microstrip model in CST with the frequency response.	25
3.23 Patch antenna model in CST.	25
3.24 Frequency response of the patch antenna in figure 3.23.	26
3.25 Parameter sweep results of the patch antenna in figure 3.23.	26
3.26 Return loss of the patch antenna before designing the feed inset.	27
3.27 Parameter sweep results of the patch antenna's feed inset.	27
3.28 Patch antenna model after designing the feed inset.	28
3.29 Possible placements of the terminations.	28
3.30 X-band via and the frequency response.	29
3.31 Final patch antenna model.	29
3.32 Simulated return loss of the final patch antenna in figure 3.31.	30
3.33 Simulated antenna pattern of the final patch antenna in figure 3.31.	30
3.34 Linear patch array and simulated coupling.	32
3.35 Simulated return loss of the linear patch array.	33
3.36 Simulated farfield pattern of the linear patch array.	33
3.37 2D patch array and simulated coupling.	34
3.38 Simulated return loss of the 2D patch array.	35
3.39 Simulated farfield pattern of the 2D patch array.	35
3.40 Single patch antenna in Altium.	35
3.41 Single patch antenna with a SMP connector in Altium.	36
3.42 Manufactured Altium PCB.	36
3.43 Manufactured patch array with visible warping.	36
3.44 First iteration of the mounting bracket.	37
3.45 Height misalignment of the first bracket.	37
3.46 First iteration of the mounting bracket.	37
3.47 Block diagram of the required test setup.	38
3.48 Reflections measured by the receiver horn antenna.	38
3.49 MATLAB script to import and normalize the $S_{21}$ to the $50\Omega S_{21}$ .	39
3.50 MATLAB script to analyze the encoded phase and the error of the AUT.	39
3.51 Smith chart with phase relative phase angles.	40
4.1 Test Setup.	41
4.2 Three different AUT used during testing.	42
4.3 Measured return loss of the design patch (AUT).	43
4.4 Measured $S_{21}$ magnitude & phase.	43
4.5 Measured and unprocessed phase difference between the open and short AUT.	44
4.6 Measured and unprocessed $S_{21}$ plotted on the smith chart.	44

4.7	$S_{21}$ normalized to the $50\Omega S_{21}$ plotted on the smith chart. . . . .	45
4.8	Encoded phase difference of the AUT normalized to the $50\Omega S_{21}$ . . . . .	45
4.9	Zoomed-in plot of figure 4.8(bottom). . . . .	46
4.10	Mean, standard deviation and phase error of first set of measurements. . . . .	47
4.11	First set $S_{21}$ (left), Second set $S_{21}$ (right). . . . .	48
4.12	Encoded phase difference of the AUT normalized to the $50\Omega S_{21}$ . . . . .	49
4.13	Mean, standard deviation and phase error of all measurements. . . . .	50

# List of Tables

3.1	Dielectric comparison.	22
3.2	Dielectric comparison.	31
4.1	Phase error of first set of measurements	46
4.2	Phase error of all measurements	49

# Abbreviations

ESA	Electronically Steered Array
VNA	Vector Network Analyzer
IC	Integrated Circuit
RF	Radio Frequency
AUT	Antenna Under Test
PCB	Printed Circuit board
SLL	Side Lobe Level
EM	Electro Magnetic
EMC	Electro Magnetic Compliance
COTS	Commercial off-the-shelf
RL	Return Loss
CPW	Coplanar Waveguide
GCPW	Grounded Coplanar Waveguide
FMCW	Frequency Modulated Continuous Wave
CAD	Computer Assisted Drawings
AP	Array Pattern
EP	Element Pattern
RMS	Root Mean Square

# Chapter 1

## Introduction

### 1.1 Background

Typical ESA's today uses one of the four main types of feed networks, namely Series, Parallel, Space-Fed and Reflective Space-Fed [1]. For all four of the feed network types the system requires a phase shifter for each antenna elements. Phase shifters are expensive devices especially at high frequency bands such as X-Band and cost well over \$100 per IC [2]. Typical ESA's consist of over a 1000 individual antenna elements such as the AN/APG-63(V)1 radar with 1500 antenna elements [3]. Each of these elements would require an expensive phase shifter.

For RF systems in general each component and microstrip line is designed to match the characteristic impedance of the system, usually  $50\Omega$ . If a transmission line has a perfectly matched load, maximum RF power will be transferred to the load. The other extreme would be an short or open load, where the minimum RF power would be transferred to the load. For ideal cases, a match load will have no reflected signal, an open load will reflect the total signal without zero phase change and the shorted load will reflect total signal with a  $180^\circ$  phase change. Reflected power is usually seen as lost power, however for a reflector array this is opposite [4].

### 1.2 Problem Statement

When designing a low-cost ESA, it would be nearly impossible to build to keep cost low due to the high number of antenna elements that each requires an expensive phase shifter. Therefor a design without phase shifters would be ideal.

### 1.3 Objectives

The objective is to design a reflector array that digitally encodes the reflector elements using PIN diode switches to switch between open load ( $0^\circ$  phase change) and short load ( $180^\circ$  phase change) for each individual antenna element. To design such a system one must first verify that it is possible to induce a fixed phase difference when changing the antenna element's load to from open to short-circuit and back again. The AUT must have a fixed or constant and predictable phase difference between the open load and short-circuit irrespective of the distance from the radiating feed antenna. Only if this possible will one be able to design the describe reflector array system.

## 1.4 System Requirements

To verify that an antenna element can be encoded with a phase shift by switching between a short and an open load an antenna is required. An X-Band patch antenna is designed with the focus on being able to change the load between short, open and matched load. 3 Different versions of the same antenna are manufactured on the same PCB as well as a 3D printed bracket the keeps the antenna in the same position when swapping the antenna loads for testing. Using the Rohde & Schwarz ZVA40 VNA and two X-Band Horn antennas, radiate the designed patch antenna (AUT) for all loads and save the S-parameters. Repeat the test at different distances in the far-field. Write **LTSBEN001\_phase\_comparison.m** that loads and normalizes all measurements to the match load measurement at each frequency point. The script further calculates the difference between the open load and short circuit measurements relative to the match load measurement at each frequency point. Repeat the test on a different day to verify the repeatability of the measurements. Verify that the patch is able to be encoded with a phase difference and identify future steps and tests required for the proposed system in section 1.3.

## 1.5 Scope & Limitations

For this investigation it is assumed that the final system will be able to calibrate out and normalize the phase measurements relative to the matched load case. The assumption is made that all the environment and common effects are captured in the matched load measurement. For this investigation it is assumed that the errors induced by swapping between 3 identical antennas will be negligible during testing. This report will only focus on whether the phase difference between the short and open load phases are constant when normalized to the matched load measurement and not how this normalization will be practically implemented.

## 1.6 Report Outline

The report will first provide the necessary information needed in the Literature Review section. The System Design is divided into two sections namely, Antenna Detailed Design and Signal Processing. The Antenna Detailed Design section provides all the design choices made during the for the AUT, while the Signal Processing section provides the required Matlab script to test and analyse the measured S-parameters. The Results section provides the results of the measurement analyses with short discussions. The conclusion provides feedback on the feasibility of the described systems in section 1.3 as well as the required future testing and development to achieve this system.

# Chapter 2

## Literature Review

### 2.1 Antenna

#### 2.1.1 Antenna Gain

An antenna is a RF device that transfers energy from closed system to free space. Antennas are usually designed to be pointed at an object, receiver, or scene. Therefor an antenna is designed to have the majority of its power radiated in the direction it's facing. This is known as the directivity of an antenna. The antenna pattern provides a visual representation of an antenna's directivity as seen in figure 2.1. The antenna main lobe includes the energy radiated in the intended direction, whereas the back lobe and side lobes include energy radiated in all other directions. The higher the side lobes, the less energy is radiated in the main lobe. Side lobes are an unavoidable byproduct of antenna design, however there are techniques to decrease the SLL (Side Lobe Level). The Antenna Gain is measured in either dBi or dBd which is the decibel level relative to a isotropic radiator or dipole respectively.

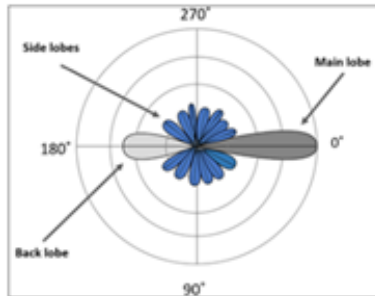


Figure 2.1: A typical Antenna pattern.

#### 2.1.2 Nearfield & Farfield

As seen in the figure 2.2, the greater the distance away from the antenna more planar the transmitted waves become. The region where the transmitted wave can safely be approximated as a planar wave is known as the Far field. The Region between the antenna and the far field is known as the nearfield region and in general radars operate in the Farfield. The Farfield distance depends on the maximum dimension of the antenna's radiating surface or aperture, [5].

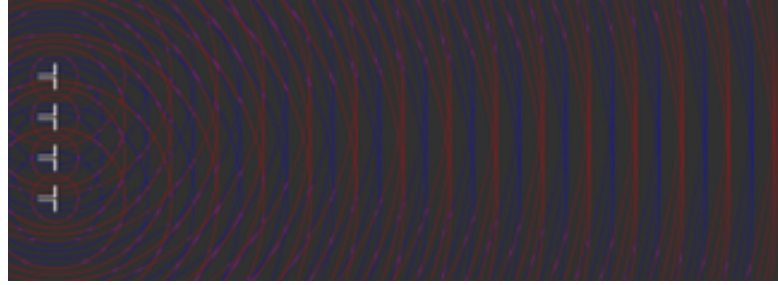


Figure 2.2: Transition from spherical waves to planar waves.

According to [5] the distance is depended on the maximum dimension of the antenna and is calculated as

$$R_{ff} = \frac{2D^2}{\lambda}$$

Most antennas are resonant structures or at the very least consist out of multiple resonant structures, meaning that they have narrow bandwidths due to some dimension of the antenna being a fraction of the signal wavelength at the center frequency ( $f_0$ ).

### 2.1.3 Monopole Antenna

One such resonant antenna is the monopole antenna. It can be built by simply cutting a cable to the resonant length, which is a quarter of a wavelength at the center frequency. A monopole does not have high directivity as it has an omnidirectional radiation pattern in azimuth, see figure below. Other forms of antennas are more complicated to design and manufacture, but they offer better directivity, allowing the operator to focus more of the energy in the direction of interest. Typical monopole antennas have a gain of 2-5 dBi.

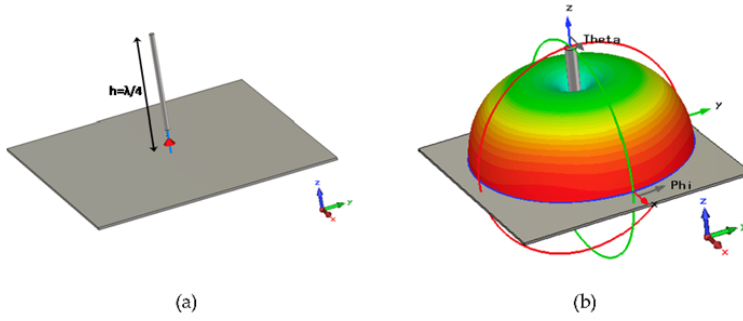


Figure 2.3: Monopole model and 3D antenna pattern.

### 2.1.4 Patch Antenna

An example of an antenna with higher directivity is a patch antenna. A patch can be designed to have gain ranging between 5-10 dBi. The patch antenna is still a resonant antenna as it has narrow bandwidths and the center frequency is determined by the length of the (L) and the substrate used, see figure 2.4. Equations see below from [6]

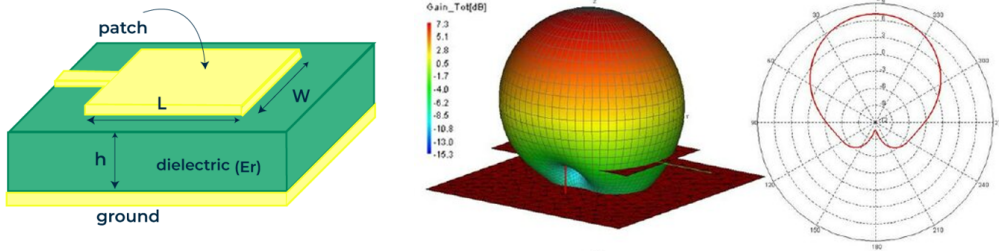


Figure 2.4: Patch antenna model and antenna pattern.

For the design equations of a patch antenna it is assumed that the thickness of the substrate is significantly smaller than a wavelength at the center frequency of the antenna. The equation becomes inaccurate if this assumption does not hold due to fringing fields, see figure 2.5. The fringing fields increase the effective length of the antenna, in turn lowering the center frequency [7].

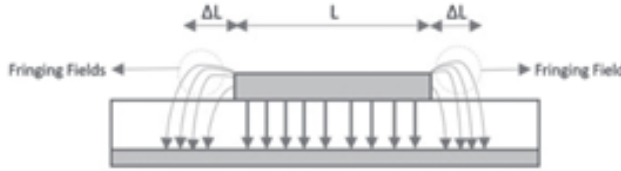


Figure 2.5: Fringing fields on a patch antenna.

The bandwidth of the antenna is determined by the width of the patch and can be calculated with the equation below.

$$B = 3.77 \frac{\epsilon_r - 1}{\epsilon_r^2} \frac{W}{L} \frac{t}{\lambda}$$

Since RF circuits are designed for a certain characteristic impedance and the edge of a patch is usually at a different impedance, the impedance must be transformed. The impedance at the edge of the patch is given by

$$Z_A = 90 \frac{\epsilon_r^2}{\epsilon_r - 1} \left( \frac{L}{W} \right)^2$$

As the antenna feed point is moved from the edge of the patch to the center of the patch, the impedance decreases until it reaches  $0\Omega$  at the middle of the patch.

$$Z_A (\Delta x_p) = Z_A (\Delta x_p = 0) \cos^2 \left( \frac{\pi \Delta x_p}{L} \right)$$

### 2.1.5 Horn Antenna

For applications where more gain is needed, aperture antennas are commonly used. One such aperture antenna is the Horn antenna as they typically have more than 15dBi of gain. The advantage of the horn antenna is the high gain and high bandwidth. The disadvantage of the horn antenna is larger physical size of the antenna.

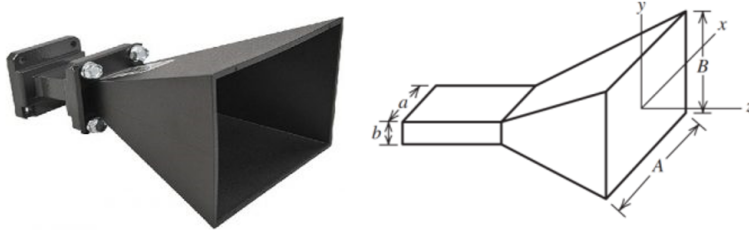


Figure 2.6: A typical horn antenna.

The gain of a pyramidal horn can be calculated as, assuming an aperture efficiency of 50%, [8]

$$G = 0.5 \left( \frac{4\pi}{\lambda^2} AB \right)$$

## 2.2 Radar Range Equation

The maximum range of a radar system depends on the transmitted power ( $P_t$ ), the received power ( $P_r$ ), the transmitter antenna gain ( $G_t$ ), the receiver antenna gain ( $G_r$ ), the wavelength ( $\lambda$ ) and the radar cross section ( $\sigma$ ), [5]. The wavelength is proportional to the transmitted wave's frequency. The radar cross section refers to the area visible from the transmitter.

$$P_r = \frac{P_t G^2 \lambda^2 \sigma}{(4\pi)^3 R^4}$$

## 2.3 Frequency bands

As the Electromagnetic (EM) spectrum is a limited resource it is divided up into different frequency bands for different wireless transmission applications. Radars tend to operate between chose the operating frequency based on the range and resolution of the planned 1-40GHz. Since the wavelength inversely proportional to the frequency, the higher the frequency the physically smaller Radar and RF equipment become. Producing accurate but smaller radars becomes more expensive due to the component cost as well as the RF test equipment needed for the development.

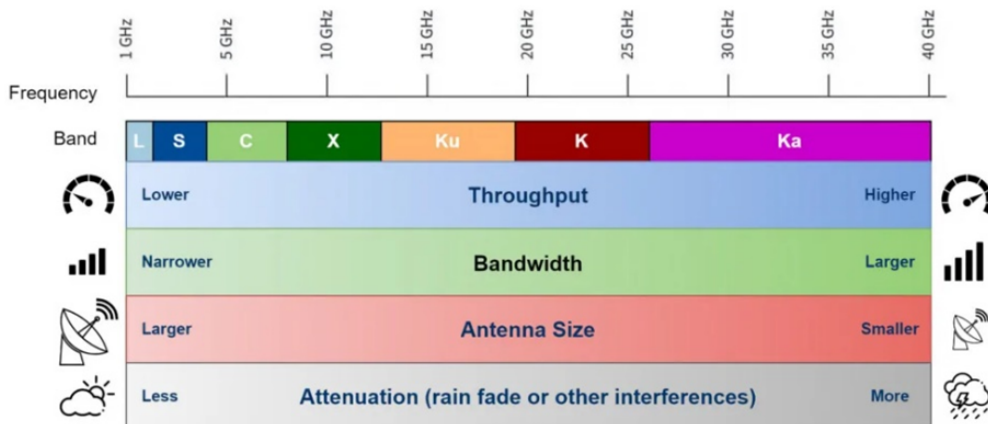


Figure 2.7: Assigned Frequency Band in the EM spectrum.

## 2.4 RF system impedance ( $50\Omega$ matched systems)

Impedance matching is a fundamental aspect of RF design and testing; the signal reflections caused by a mismatched impedance can lead to unwanted behavior and losses. The standardized RF impedance is  $50\Omega$ , but it is important to understand that any other impedance can be used, but most COTS RF components are designed for  $50\Omega$  systems, [9].

In a closed  $50\Omega$  system between each of the components the quality of the match (how close to  $50\Omega$  to component is) is characterized by an input Return Loss ( $RL_{in}$ ) and an output Return Loss ( $RL_{out}$ ). The worse the match the more power is reflected back in the opposite direction of propagation, i.e. power lost. The worst RL possible is either an open circuit ( $\infty\Omega$ ) or a short circuit ( $0\Omega$ ). Both an open and short circuit reflects all the power, however a short circuit reflects the signal with a change in phase of  $180^\circ$ . An open circuit reflects the signal without a change in phase, see figure 2.8, [4].

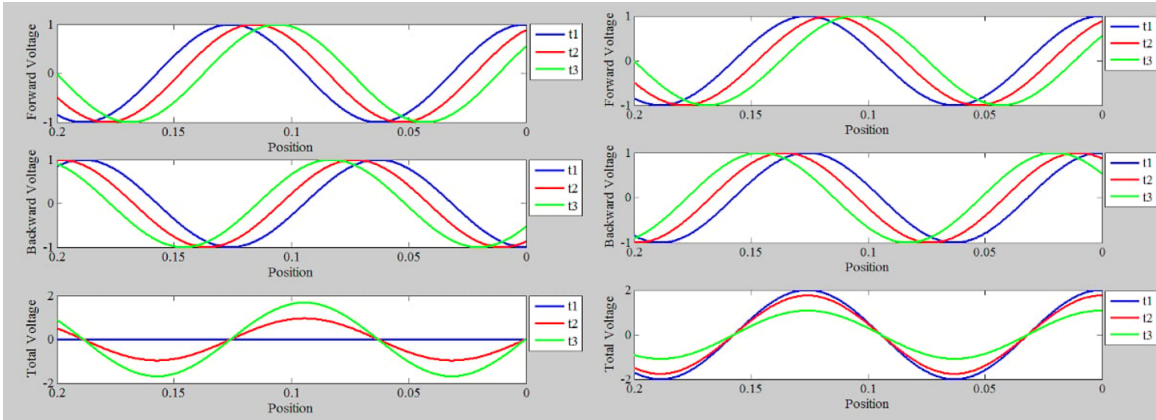


Figure 2.8: Reflection of a sinusoidal wave at an open circuit (left) and short circuit (right).

### 2.4.1 Smith Chart

The smith chart is a useful tool for RF design. It provides a visual method to characterize the impedance of RF components and transmission lines. A short perfect  $0\Omega$  would be plotted on the far left of the chart, a perfect  $50\Omega$  would be plotted at the origin and a perfect open circuit would be plotted on the far right of the smith chart. The smith chart also allows the designer to determine what type of impedance transformation is needed as seen in the figure 2.9.

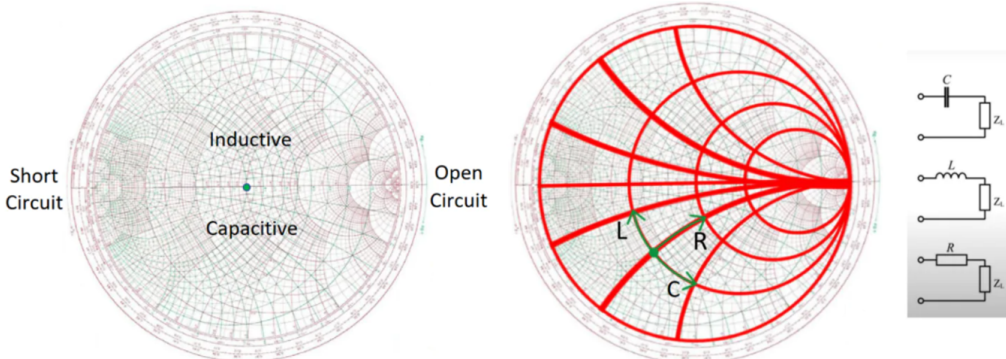


Figure 2.9: Smith chart and how lumped element move on the smith chart.

## 2.5 Dielectric materials

Printed Circuit Boards (PCB) consist of multiple electrically conductive layers. The substrate separates these electrically conductive layers is known as a dielectric. Multiple dielectric types exist and choosing the dielectric effects the entire RF design. The width for a  $50\Omega$  trace on a PCB depends on the type of dielectric as well as the thickness of the chosen substrate.

FR4 is the most common dielectric, but it is very lossy when used at high frequencies [10]. High frequency PCB uses more expensive dielectric materials such as Rogers RO4003C, which have much lower losses at high frequencies, but cost 10 times more .

In free space a signal propagates at the speed of light ( $c_0$ ), however in a dielectric medium the velocity of propagation is decreased by a factor of  $\frac{1}{\sqrt{\epsilon_r}}$  . The effect is also observed with the wavelength decreasing in the dielectric and can be mathematically described below, [11].

$$\lambda = \frac{c}{f\sqrt{\epsilon_r}}$$

### 2.5.1 PCB Transmission lines

Many different types of transmission lines can be designed for RF trace on and within a PCB. The most common is microstrip and its impedance can be calculated as

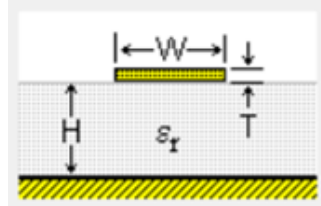


Figure 2.10: Microstrip model.

$$Z_0 = \frac{87}{\sqrt{\epsilon_r + 1.41}} \ln \left( \frac{5.98H}{0.8W + T} \right)$$

Other common types include Stripline, Coplanar Waveguide (CPW) and Coplanar Waveguide with ground (GCPW). A visual representation of all there can be seen in figure below. Each transmission line type becomes more elaborate to calculate the impedance of the trace, fortunately the dielectric manufacturers tend to provide calculator tools to calculate the impedance.

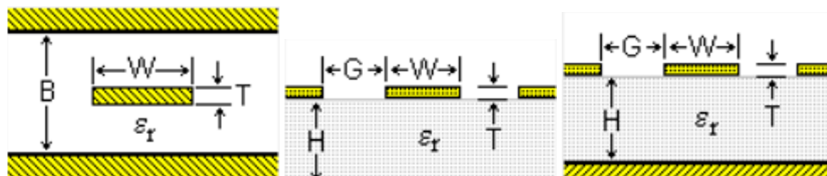


Figure 2.11: Stripline model (left), CPW model (middle) and GCPW model (right).

### 2.5.2 Coaxial Cables

Another type of RF transmission line that is commonly used for RF cables is the round Coaxial transmission line. These coaxial cables are usually sold as  $50\Omega$  or  $75\Omega$  cables.

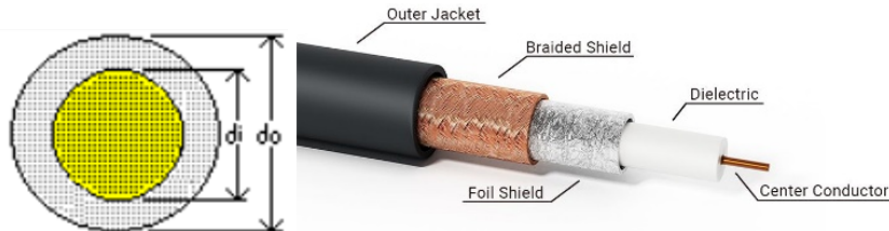


Figure 2.12: Coaxial Cable.

## 2.6 FMCW

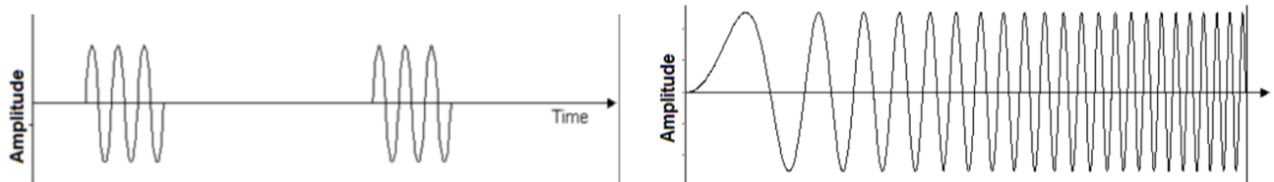


Figure 2.13: Pulsed waveform (left), FMCW waveform (right).

Two main types of radars exist, pulsed radars and continuous wave radars. A pulsed radar transmits a pulse and waits for the reflected pulse. Since the radar only transmits for a short period, the radar can transmit a high-powered pulse. This ensures a large maximum range for the radar. The duty cycle of the radar refers to the ratio of transmit time to the total time. Usually, the larger the transmitted power is, the shorter the pulse will be. This is to reduce the total power draw during operations. Unfortunately, the radar is blind while waiting for the returned pulse [12]. A pulsed radar usually operates at a single frequency lower than 50kHz. A Frequency Modulated Continuous Wave (FMCW) radar transmits continuously, and therefore at lower power than a pulse radar. The maximum range is thus also lower, but the radar is never blind. The waves frequency is varied when transmitting, this is done to differentiate the received signal and determine the propagation delay [12]. The frequency sweep of a FMCW radar can either be sweep up or sweep down with a large frequency range, typically from 1GHz to 40GHz.

## 2.7 RF simulation software

To complex RF components & antennas becomes a computationally intensive exercise. Many software suites are available to solve the EM performance of a designed 3D model. To two software suites available at the time of this report were Altair FEKO and Dassault Systèmes CST Studio Suite.

### 2.7.1 FEKO

FEKO is commonly used for antenna design, the Farfield performance of a designed structure as well as EMC compliance. FEKO is easy to understand with a minimal learning curve when designing antennas, however its UI is still limited at the time of the report. The minimum mesh size is much larger than CST Studio, however there are methods to force a smaller mesh at certain places by adding a second slightly smaller copper block over an existing copper block. FEKO's parameter sweep macro runs on a CMD window and creates a separate CAD model for each parameter change which is solved individually. The results cannot be viewed together, unless the entire parameter sweep has run successfully and the .xml file was automatically generated.

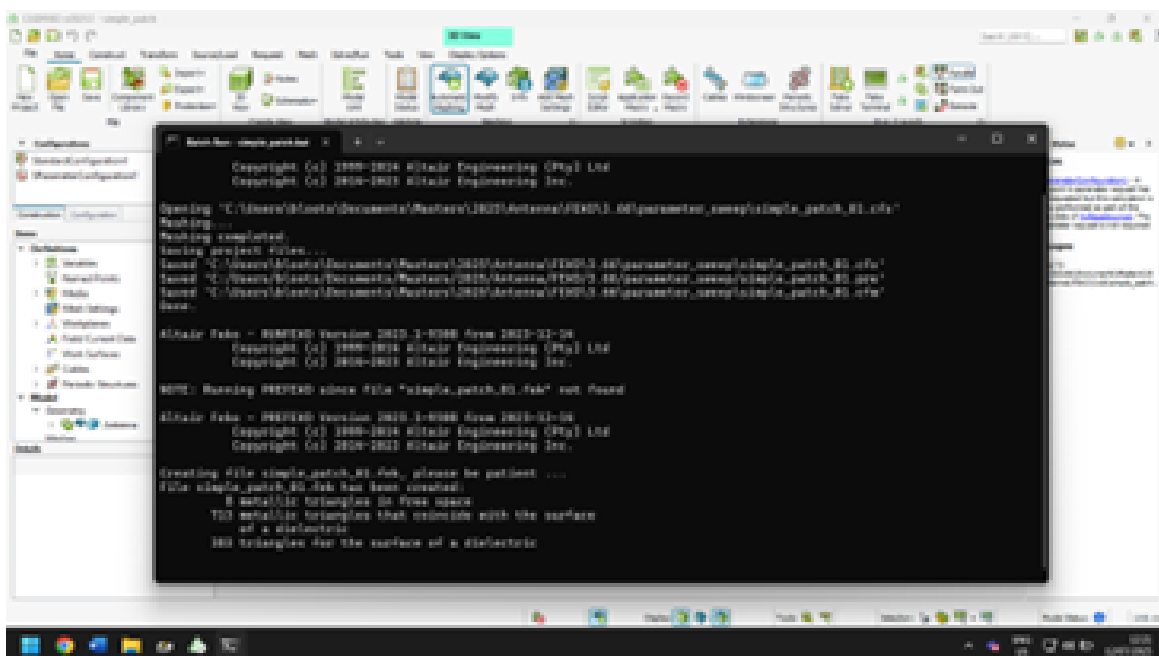


Figure 2.14: Running a parameter sweep in FEKO.

FEKO also provides more port options and source options. An edge port is very simple to implement for a microstrip line, but not for a CPW line. The help documentation is quite limited.



Figure 2.15: Available ports and sources in FEKO.

### 2.7.2 CST

CST Studio on the other hand has a steeper learning curve, but a much more extensive UI and help documentation. CST Studio only uses two port types, but the waveguide port can be used for most feeds including microstrip, stripline and CPW. CST also provides a macro that constructs the port correctly on the picked face.



Figure 2.16: Available ports and sources in CST.



Figure 2.17: Port extension coefficient macro in CST.

As for the parameter sweeps, CST automatically lists all the versions together and if the parameter sweep was cancelled before it was completed, all the completed runs can still be viewed in the same manner.

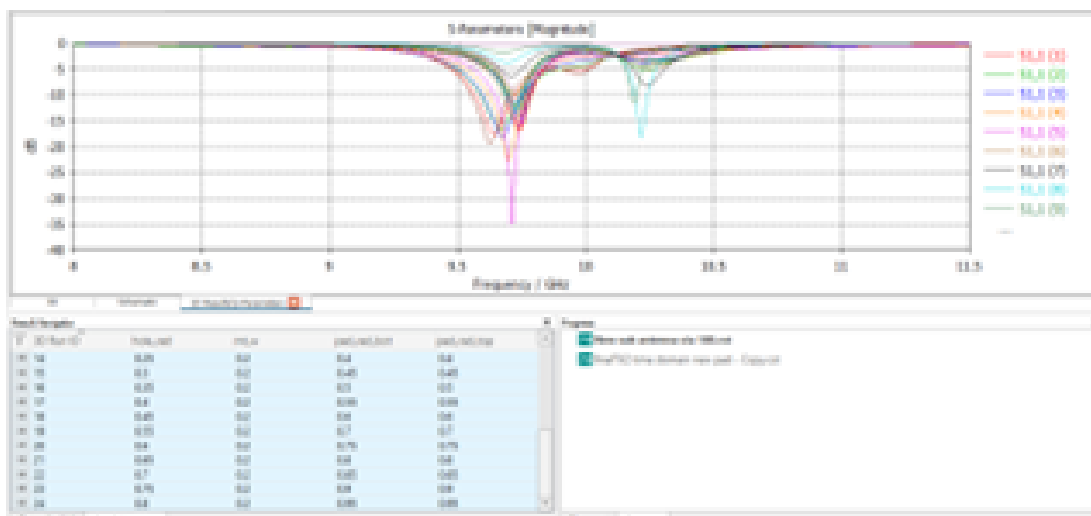


Figure 2.18: Parameter sweep in CST.

In industry FEKO is used for Farfield simulations such as antennas and CST is preferred for nearfield simulations such as X-Band vias and transitions. Keep in mind they are both capable of solving both nearfield and Farfield designs .

## 2.8 ESA

For a radar to measure the angle of a target more than one antenna is required, since the delay ( $\Delta d_2$ ) is used to determine the angle ( $\theta$ ) of the target. The delay ( $\Delta d_2$ ) is measured as a phase delay and the phase can be converted to an angle of arrival using trigonometry.

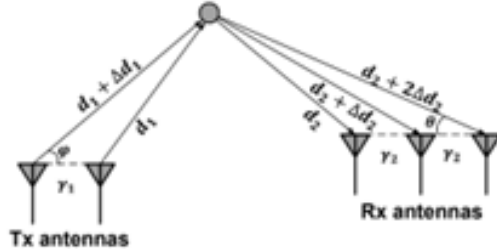


Figure 2.19: Angle extraction setup.

For the Tx antennas, a phase difference can be induced for each antenna which will then steer the main lobe in some direction ( $\Phi$ ). This is known as beam steering. Beam steering is commonly used in Electronically Steered Arrays (ESA). These ESA typically consist of over 1000 individual antenna elements such as the AN/APG-63(V)1 radar with 1500 antenna elements [3].

### 2.8.1 ESA Feeds

Each antenna element for ESA requires a feed. These feeds usually include some gain control and a phase shifter. Four main types of feed networks exist namely Series, Parallel, Space-Fed and Reflective Space-Fed [1].

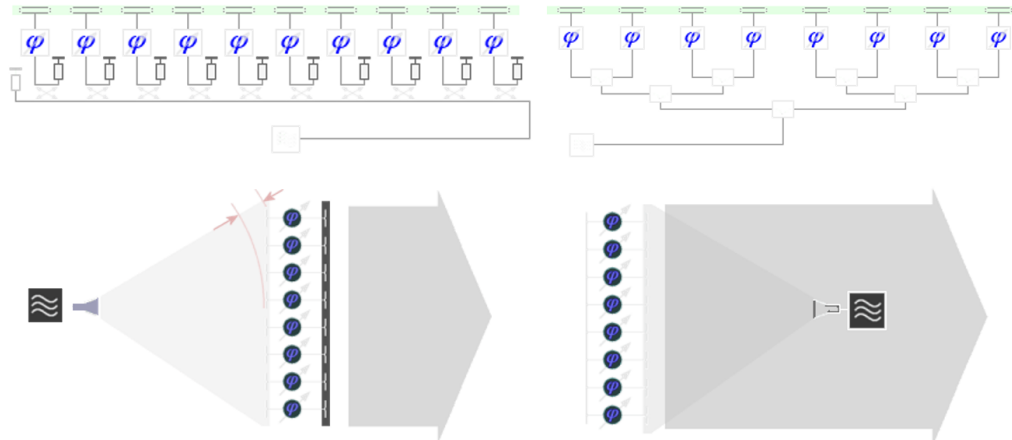


Figure 2.20: Four types of ESA feeds.

## 2.9 Permittivity and Permeability

A material's electrical and magnetic characteristics can be partially defined by its permittivity and permeability. Permittivity is the ability of a material to store electrical potential energy under the influence of an electric field measured by the ratio of the capacitance of a capacitor with the material

as dielectric to its capacitance with vacuum as dielectric [13]. Permeability is the property of a magnetizable substance that determines the degree in which it modifies the magnetic flux in the region occupied by it in a magnetic field [14].

## 2.10 VNA

A Vector Network Analyzer uses advanced electronics and signal processing to analyse the system connected to the available ports. A VNA sends test signals sweeping through frequencies and measures the results at the available ports. The results are typically recorded as scattering parameters. A 2-port VNA will return a scattering matrix as shown below [15].

$$\begin{bmatrix} S_{11} & S_{12} \\ S_{21} & S_{22} \end{bmatrix}$$

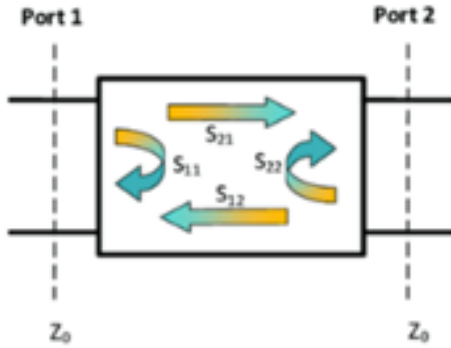


Figure 2.21: Scattering parameters diagram.

The subscripts refer to the port which received the signal and the port from which the signal is sent. Thus, the  $S_{11}$  parameter is the reflection coefficient for port 1. For a radar system the  $S_{21}$  parameter is important since it is the result at port 2 for a signal sent from port 1.

# Chapter 3

## System Design

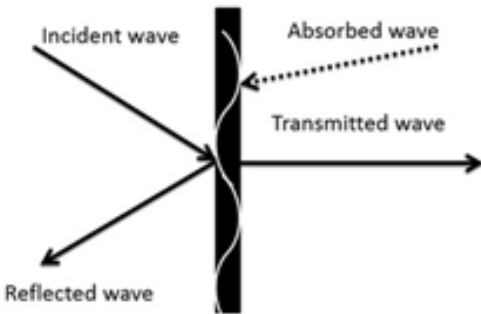


Figure 3.1: Wave incident at a dielectric boundary.

Figure 3.1 above shows the different waves present when a wave is incident at a dielectric boundary. The hypothesis for the proposed system in section 1.3 is that the absorbed wave induces currents on the reflector array. Then these induced currents cause the reflector array elements to re-radiate the majority of the absorbed wave again. If it is assumed that this is true, the goal is to then encode the re-radiated wave with a phase difference by changing the termination of the reflector array elements from and open to a short circuit and back. To verify if this is possible an antenna is designed and 3 different versions of the designed antenna is manufactured. Each version only changes load connected to the antenna.

### 3.1 Simulation based investigation

The initial investigation was planned to be simulation based and due do the ease of Farfield simulations in FEKO, the investigation started in FEKO. However, after many complications two major changes were made. Firstly, the final investigation changed from simulation based to physical measurements due to the required simulation model becoming too complex to implement in FEKO. The Planar wave source is not bounded with a specific beamwidth and the Farfield monitors do not measure the S21 parameter.

Secondly, the antenna design moved from FEKO to CST Studio, due to the complex microstrip design required. The stack-up changed to asymmetrical stack-up, which required an X-band via as well.

This section documents the obstacles and restrictions faced when trying to complete the investigation

based only on simulations.

### 3.1.1 Antenna design and ports in FEKO

FEKO provides different port setups, including wire, edge and waveguide ports. It is not clear which port is ideal for the antenna model. The waveguide port requires a waveguide structure in the model to be able to use. The antenna model seen in figure 3.2 below does not have a waveguide structure. The remaining port options are wire and edge ports.

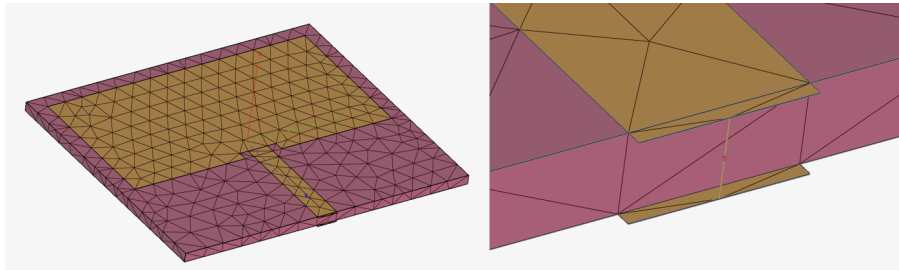


Figure 3.2: Patch antenna model in FEKO using a wire port.

The figure 3.2 above uses a wire port with a voltage source. Using the wire port requires the  $50\Omega$  trace to extend past the edge of the board and then assigning a wire radius to the wire port. There is no clear documentation for how to define the distance the trace should extend or how to determine the required wire radius. Figure 3.3 shows the return loss of -12dB at a center frequency of 9.5GHz.

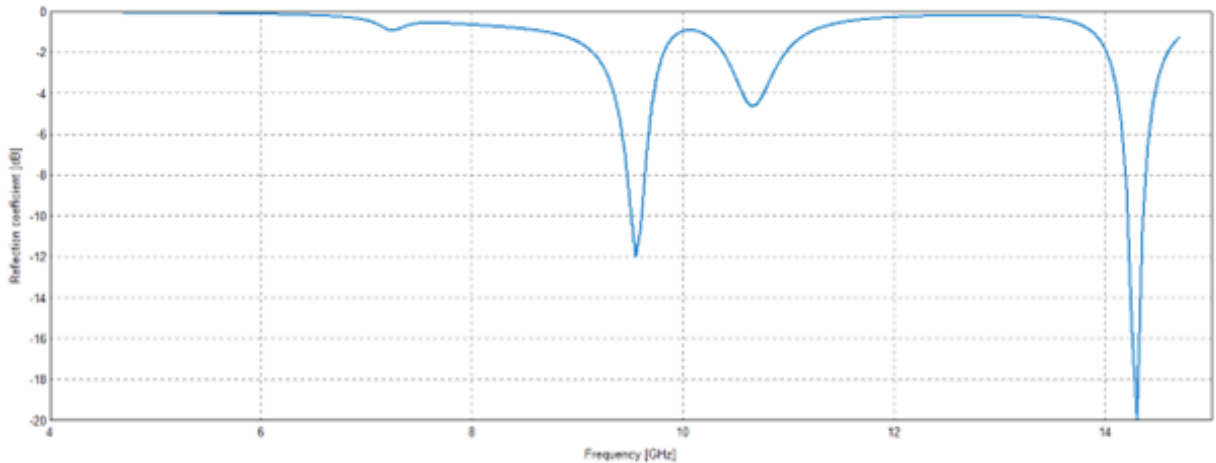


Figure 3.3: Return loss of the patch in figure 3.2

The figure 3.4 show the Farfield pattern at the center frequency of the antenna. Since gain of 5.9dBi is observed, it can be concluded that the wire port is setup correctly, however the frequency response at frequencies greater than 14GHz seem inaccurate.

### 3.1. Simulation based investigation

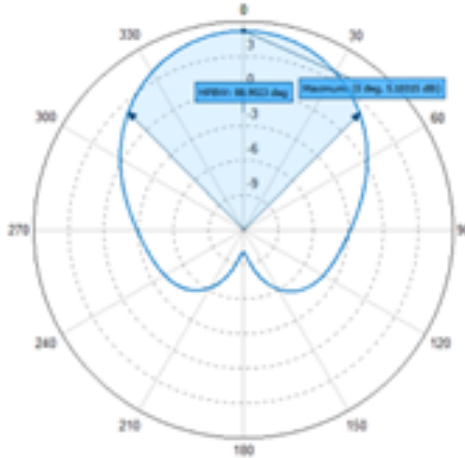


Figure 3.4: Antenna pattern of the patch in figure 3.2

The figure 3.5 uses an edge port with a voltage source. Using the edge port also requires the  $50\Omega$  trace to extend past the edge of the board however no wire radius is required. Therefor removing one of the uncertainties. Figure 3.6 shows the return loss of  $-24\text{dB}$  at a center frequency of  $9.5\text{GHz}$ , which is an significant improvement over the wire port model. The frequency response at frequencies greater than  $14\text{GHz}$  seem more realistic. From these results it is assumed that is edge port feed is more accurate for this model, however the only way to verify is to build and test the antenna.

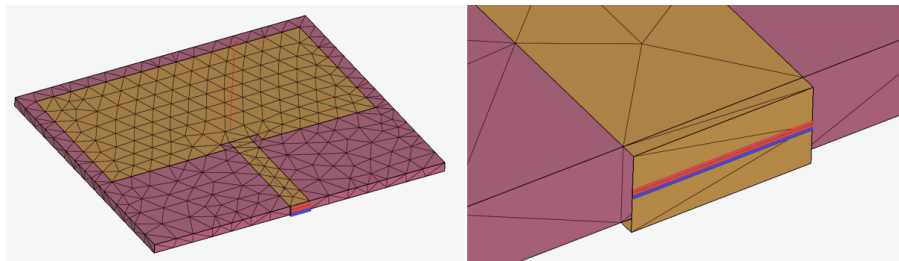


Figure 3.5: Patch antenna model in FEKO using a edge port.

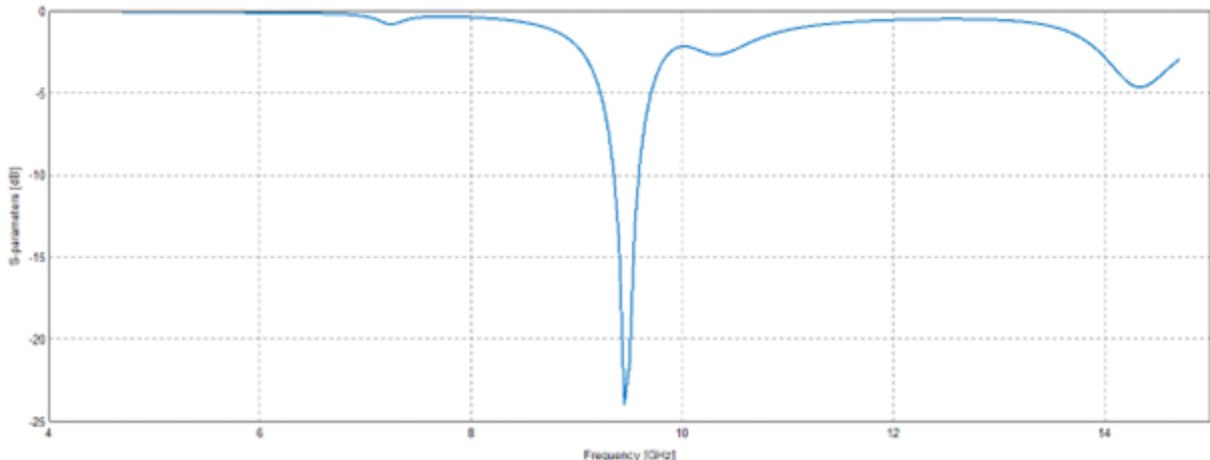


Figure 3.6: Return loss of the patch in figure 3.5

### 3.1.2 Phase & Planar wave & Dipole monitor

The next step is to radiate the patch antenna (AUT) with a RF signal and measure the phase of the reflected signal. The approach was to use FEKO's planar wave source to radiate the AUT and then place a dipole in the Farfield with a wire port. To connect a load to the antenna, a port is required on the antenna as well. This load is varied from  $0\Omega$  to  $50\Omega$  to  $10M\Omega$ .

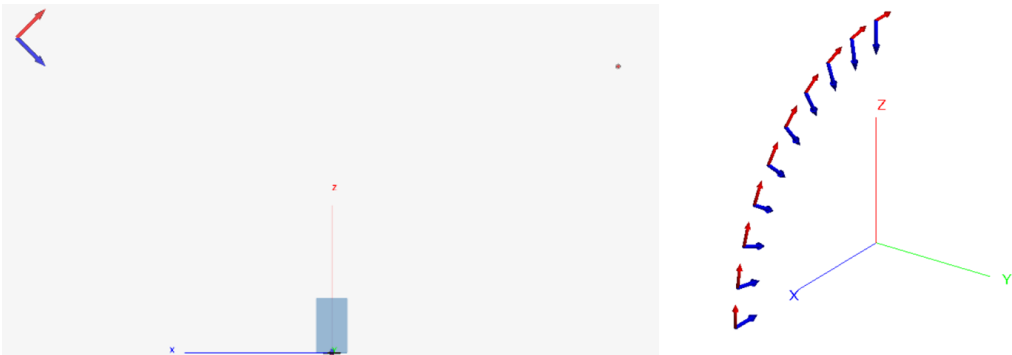


Figure 3.7: FEKO simulation setup using a dipole with a wire port as the monitor.

The figure 3.7 show the planar wave source in the top left corner, the AUT in the middle and the dipole in the top right corner. Figure 3.7 shows the planar wave source swept from  $0^\circ$  to  $90^\circ$ . One problem with this approach is that the planar wave source is not bounded and radiates the dipole as well, see figure 3.8. The dipole is omnidirectional and will absorb the planar wave. One solution to this is to use an antenna to radiate the AUT, however the simulation model becomes exponentially more complex to run.

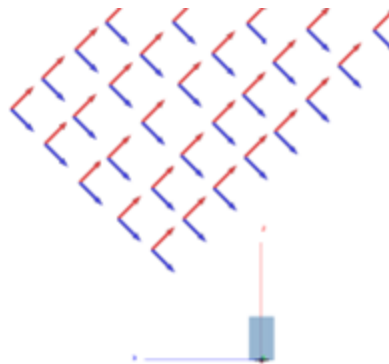


Figure 3.8: Visual representation of the unbounded planar wave source in FEKO.

An alternative approach is to use the Farfield result to measure the theoretical received phase if an receiver where to be place in the Farfield. Figure 3.9 below shows the planar wave source swept from  $0^\circ$  to  $90^\circ$  in red and the Farfield monitor setup from  $90^\circ$  to  $180^\circ$ . With this approach FEKO already calibrates out the phase from the planar wave source. This is verified by removing the AUT and observing a constant  $0^\circ$  phase in the Farfield E-field phase.

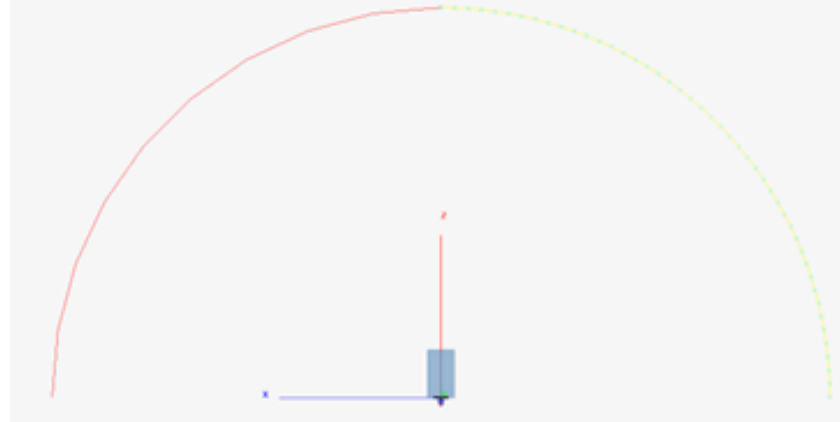


Figure 3.9: FEKO simulation setup using a farfield monitor.

Part of the simulated investigation is to see if the feed length changes the phase response. Using the model in figure 3.10 and changing the feed length would also change the ground plane size. Changing the ground plane size or the physical AUT structure that the planar wave radiates will change the phase response due a larger reflective surface. However, to observe the phase change due to the absorbed wave propagating in the feed, the physical AUT structure that the planar wave radiates must remain fixed. One way to achieve this is to use a trough hole feed and a coaxial structure behind the antenna that can change in length. This approach has a similar problem as seen in figure 3.8, where the planar wave will reflect off the coaxial cable to the planar wave not being bounded to the top of the AUT.

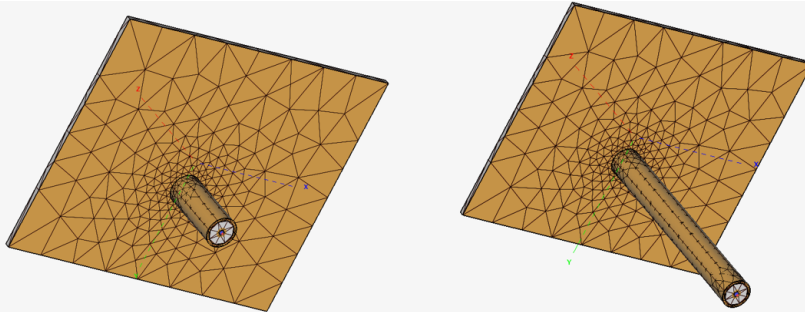


Figure 3.10: Patch antenna model with a variable coaxial cable

### 3.1.3 Coax & CPW

Simulating the model in figure 3.10 results in a extremely poor return loss. The port type was changed to verify that the port setup is not the source of the poor return loss, however the return loss remained worse than -12dB for all port types used. After many failed attempts of trying to improve the match a very simple  $50\Omega$  microstrip model was created to verify that that simulates correctly. Figure 3.11 show the microstrip model along with the simulation results. The result is indeed a  $50\Omega$  matched microstrip.

### 3.1. Simulation based investigation

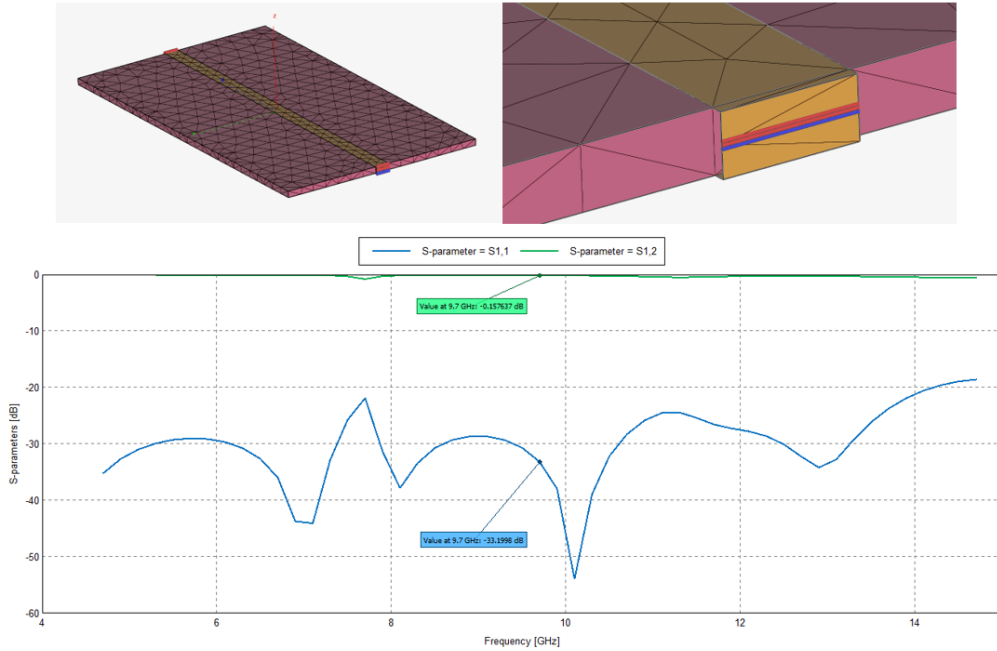


Figure 3.11: Microstrip model in FEKO using a edge port along with the frequency response.

Next a simple  $50\Omega$  CPW model was created to verify that that simulates correctly. Figure 3.12 below show the CPW model along with the simulation results. The return loss at X-Band is very poor.

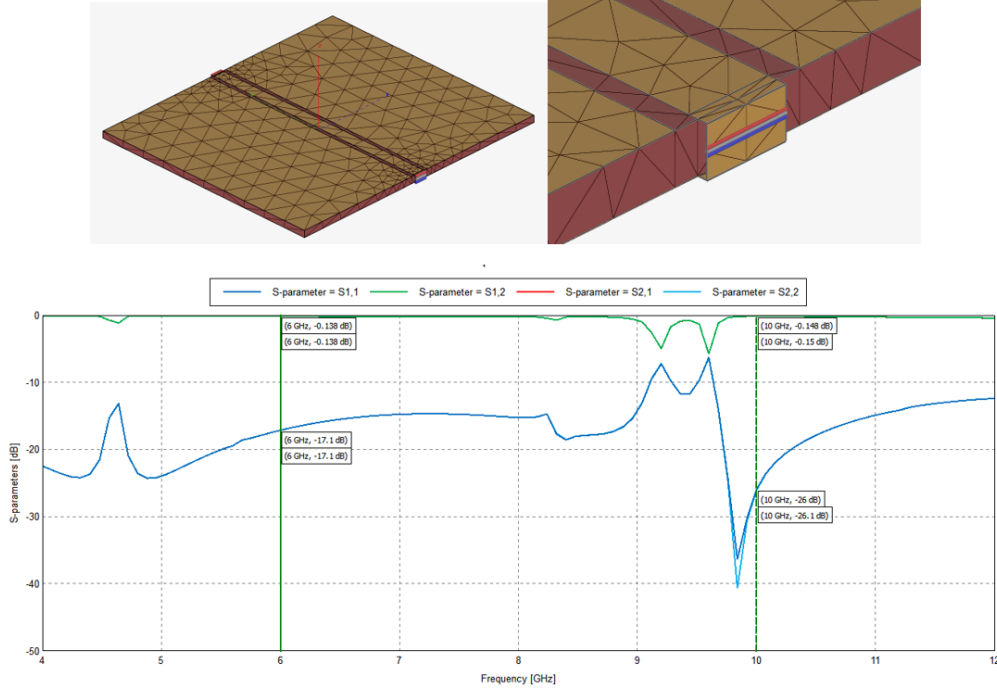


Figure 3.12: CPW model in FEKO using a edge port along with the frequency response.

Assuming that the edge port is not correct due to the port not making contact with the ground planes either side of the trace, Altair support was contacted for assistance. The model was revised base based

### 3.1. Simulation based investigation

on the comments from Altair and the model is seen in figure 3.13. The port now involves a larger copper plane that touches the bottom ground layer, the trace and the ground plane on both sides of the trace. Furthermore, a small section of the PCB needs to be cut away since the edge port cannot be place on the edge of a dielectric medium.

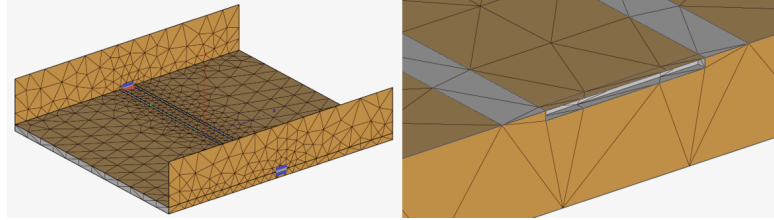


Figure 3.13: CPW model in FEKO using the supplied port from Altair support.

Figure 3.14 show the wide band response of the CPW model and a good match is observed at 7.2GHz, however a very poor match is observed at X-band. This exact CPW structure has successfully been used in radar design in the past. Figure 3.15 shows a zoom-in frequency response. That specific radar operated form 9.2 to 9.75GHz with very little losses. Knowing this the results still seem inaccurate.

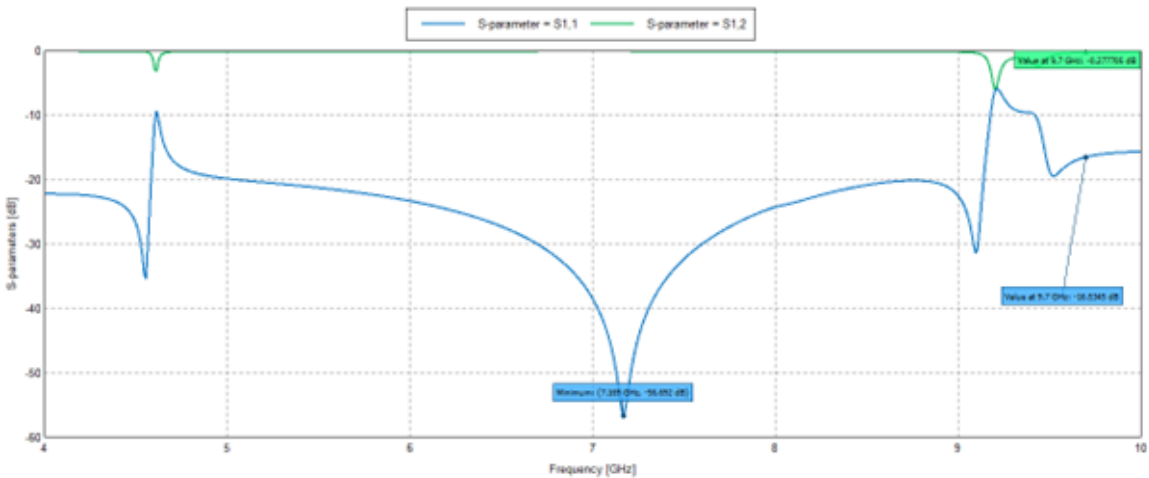


Figure 3.14: Frequency response of the CPW model in figure 3.13

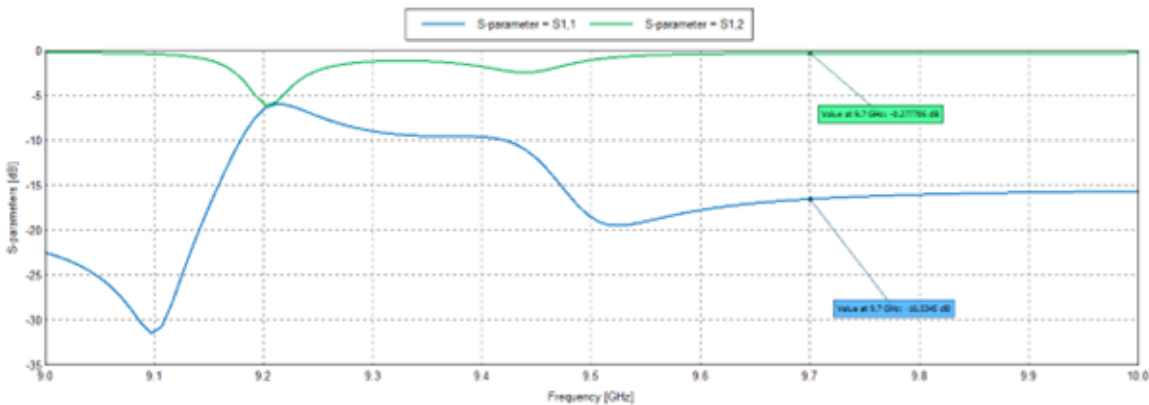


Figure 3.15: X-band frequency response of the CPW model in figure 3.13

### 3.1.4 CST Studio

The decision was made to move to designing the antenna in CST Studio and manufacturing the antenna to continue the investigation.

Firstly, the very same simple  $50\Omega$  CPW model was created to verify that that simulates correctly. Figure 3.16 show the CPW model in CST Studio. Figure 3.17. The result is indeed a  $50\Omega$  matched microstrip, see figure 3.19.

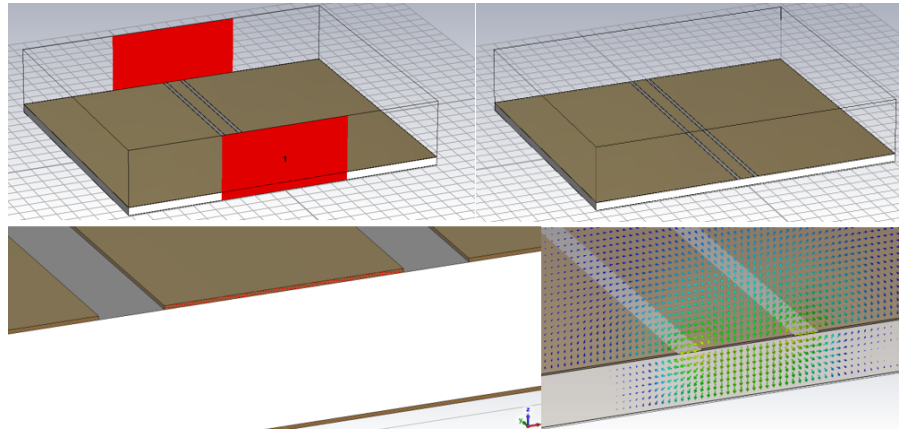


Figure 3.16: CPW model in CST using waveguide ports.

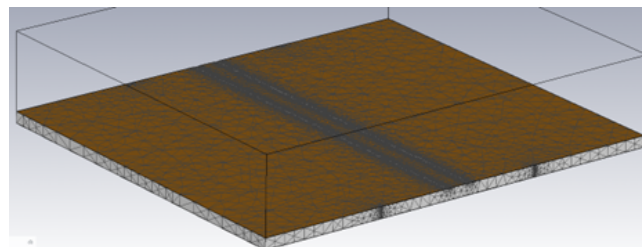


Figure 3.17: Meshed CPW model in CST.

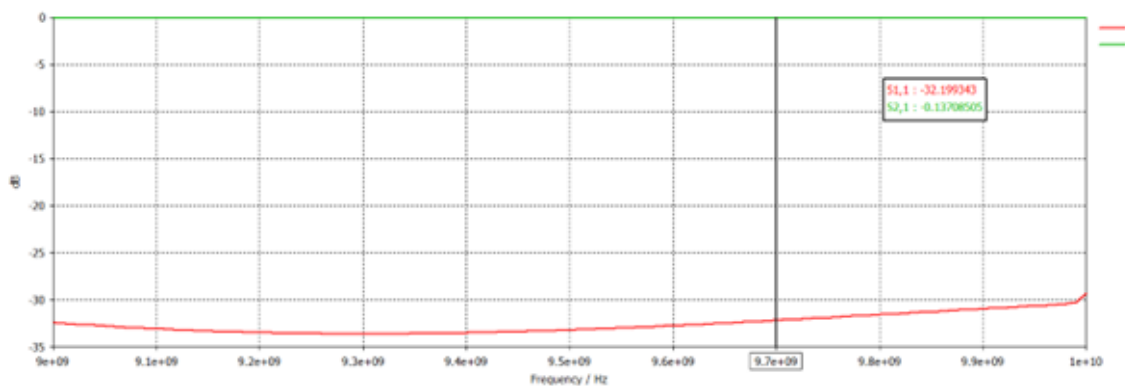


Figure 3.18: X-band frequency response of the CPW model in figure 3.16

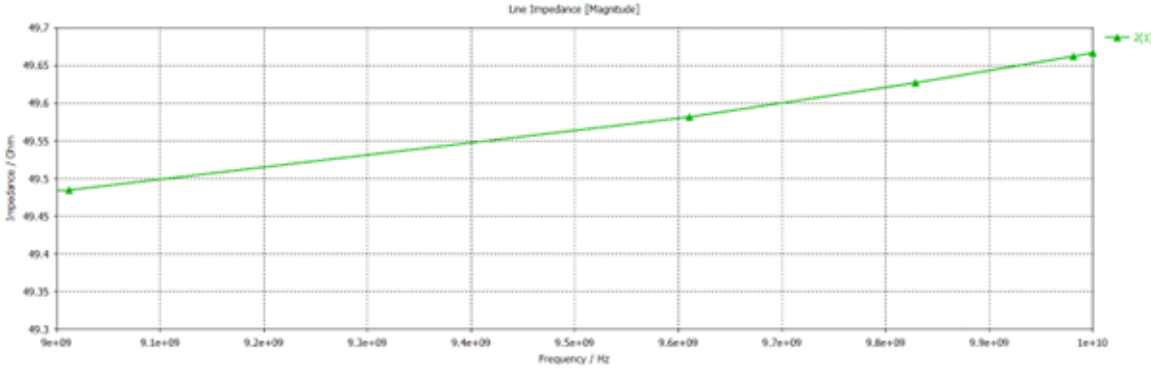


Figure 3.19: Line impedance of the CPW model in figure 3.16.

## 3.2 Antenna Detail Design

### 3.2.1 Center frequency

The antenna is chosen to be a X-Band antenna as this results in a very small antenna element and therefore a relatively small reflector array if these antennas were to be used for future testing. Due to the antenna element being small, the far-field distance remains short enough to be able to test in the laboratory with a VNA. The center frequency is chosen as 9.7GHz as this is the center frequency of an existing radar and could be used to test the final proposed system in the future.

$$\lambda = \frac{c_0}{f_c} = \frac{c_0}{(9.7GHz)} = 30.91 \text{ mm}$$

### 3.2.2 PCB Stack-up

A FR-4 substrate will be very lossy at X-band [16]. Rogers RO4003C is common substrate used for X-band applications as the Dissipation Factor ( $\tan\delta$ ) or Loss Tangent ( $D_f$ ) is significantly lower than FR-4.

Table 3.1: Dielectric comparison.

Parameter	FR-4	RO4003C
Dk	4.35 @ 500MHz	3.38 @ 10GHz
Df	0.017 @ 500MHz	0.0027 @10GHz

To mask the feed of the individual antenna elements the feed must be on the back of the PCB with a solid ground plane separating the feed and the patch. Therefore a minimum of 3 layers is required. The final stack-up is seen figure 3.20

### 3.2. Antenna Detail Design

#	Name	Material	Type	Thickness	Dk	Weight	Df
	Top Overlay		Overlay				
1	Top Surface Finish	DIG (Direct Immersion Gold)	Surface Finish	0.005mm			
1	Top Layer	18u + Plating	Signal	0.035mm		1oz	
	Dielectric 1	RO4003C	Core	0.203mm	4.1		0.0037
2	Layer 2	No Copper Required	Signal	0.001mm		1oz	
	Dielectric 2	RO4450F	Prepreg	0.102mm	4.8		0.02
3	Layer 3	35u	Signal	0.035mm		1oz	
	Dielectric 3	RO4003C	Core	0.203mm	4.1		0.0037
4	Bottom Layer	18u + Plating	Signal	0.035mm		1oz	
	Bottom Surface Finish	DIG (Direct Immersion Gold)	Surface Finish	0.005mm			
	Bottom Overlay		Overlay				

Figure 3.20: PCB stackup used for the antenna design.

If the third layer is used for the ground plane, then the second layer is not required. By removing the copper from the second layer the substrate height increases as the substrate now consists of both the RO4450F and RO4003C. This increase in substrate height will increase the bandwidth of the antenna due to an increase in fringing fields [7].

Rogers provides a Microwave Impedance Calculator tool to calculate the dielectric properties for a given stack-up and frequency. The composite dielectric constant at 9.7GHz is calculated as 3.78 using the tool, see figure 3.21.

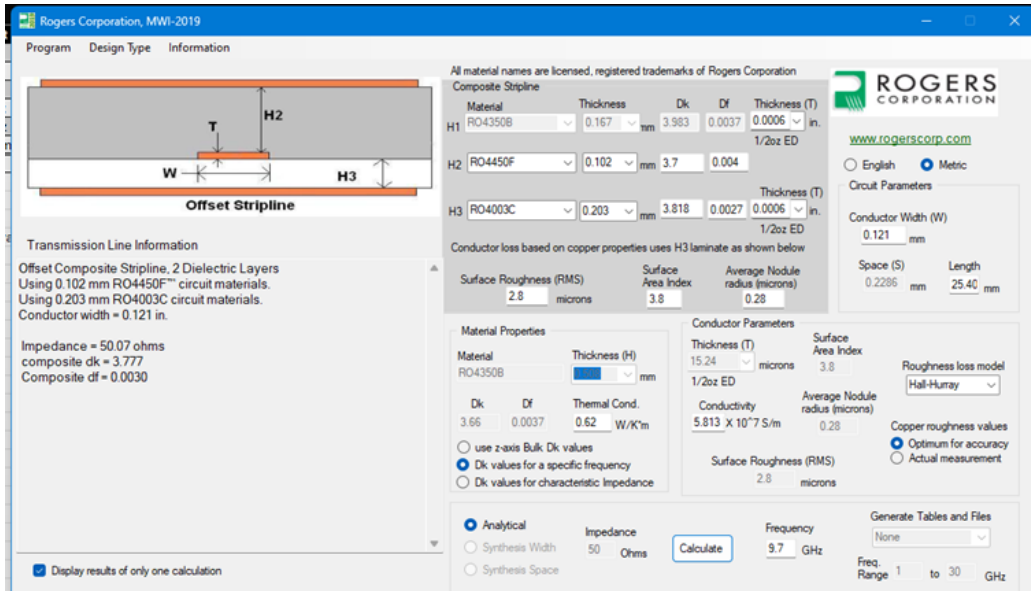


Figure 3.21: Roger Corporation's Microwave Impedance Calculator.

#### 3.2.3 Patch Dimensions

The patch length for a half wave patch antenna is calculated as follows [6]. This is an approximation and will need to be tuned during simulations.

$$f_c \approx \frac{c_0}{2L\sqrt{\epsilon_r}}$$

### 3.2. Antenna Detail Design

$$L \approx \frac{c_0}{2f_c\sqrt{\epsilon_r}} = \frac{c_0}{2(9.7GHz)\sqrt{3.78}} = 7.95mm$$

The bandwidth of the antenna is determined by the width of the patch. The radar mentioned in section 3.2.1 has a 150MHz bandwidth and the antenna is designed to match the radar's bandwidth. The patch width is calculated as follows. This is an approximation and will need to be tuned during simulations.

$$B_{-10dB} = 3.77f_c * \frac{\epsilon_r - 1}{\epsilon_r^2} * \frac{W}{L} * \frac{t}{\lambda}$$

$$W = \frac{\epsilon_r^2 * L * \lambda * B}{3.77 * (\epsilon_r - 1) * t * f_c}$$

$$W = \frac{(3.78)^2 (7.95mm)(30.91mm)(150MHz)}{3.77 (3.78 - 1) (0.305mm)(9.7GHz)} = 16.98mm$$

The size of the ground plane width ( $W_g$ ) must be sufficiently large that the fringing fields do not exceed the edges of the ground plane. Since fringing fields are proportional to the substrate height, the distance from the edge of the patch to the edge of the ground plane ( $\Delta_g$ ) needs to be significantly larger than the substrate thickness to ensure that fringing fields do not exceed the edges of the ground plane.  $\Delta_g$  is designed to be approximately 10 times larger than the substrate thickness ( $t$ ).

$$\Delta_g \gg t, \quad \Delta_g \gg 0.305mm$$

$$\Delta_g \approx 10 * t \approx 10(0.305mm) \approx 3.05mm$$

$$W_g = W + \Delta_g = 16.98 + 3.05 = 20.03 \approx 20mm$$

The ground plane length ( $L_g$ ) needs to be large enough to fit the feed and an arbitrary length of 25mm is chosen but can be increased if needed when the feed is designed.

$$L_g > L + \Delta_g$$

$$L_g > 11mm$$

$$L_g \approx 25mm$$

The final parameter needed for the initial simulation is  $50\Omega$  trace width. This is calculated again using the Microwave Impedance Calculator tool, but the *Design Type* is changed to microstrip, and the dielectric constant is manually changed to the calculated composite dielectric constant. The  $50\Omega$  trace width is 0.681mm.

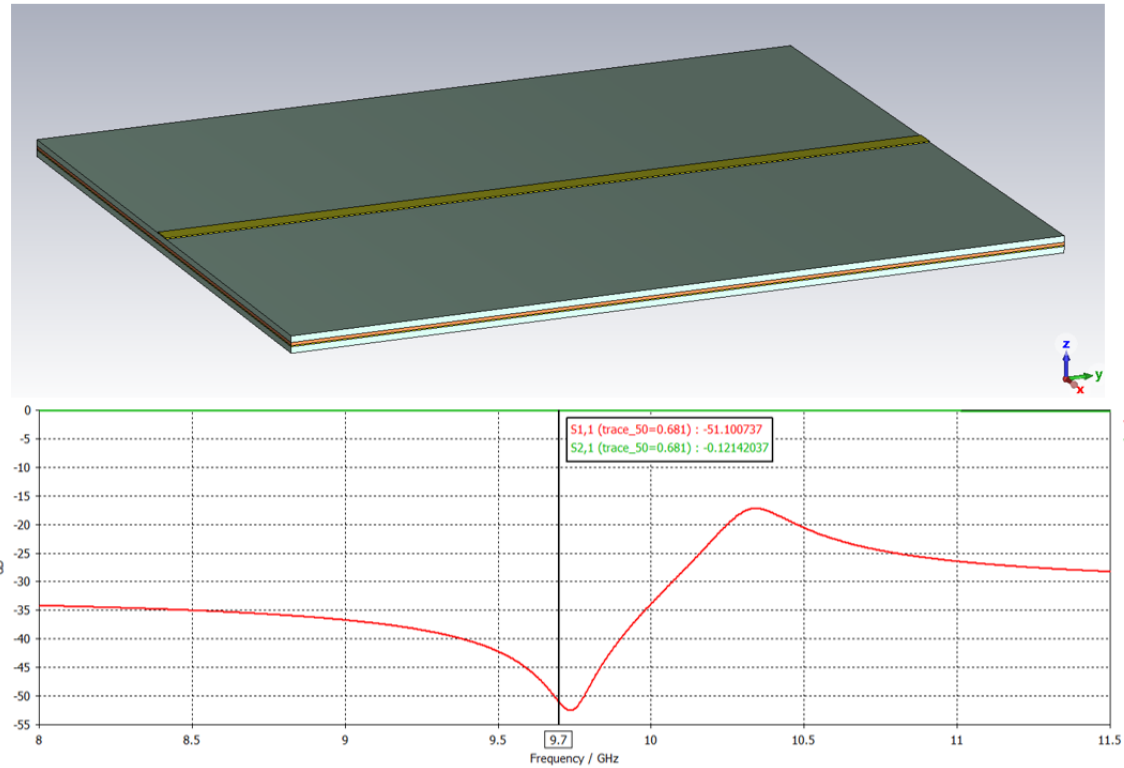


Figure 3.22: Microstrip model in CST with the frequency response.

Due past difficulty with simulation software, the  $50\Omega$  trace is simulated to verify the PCB model is setup correctly. Figure 3.22 shows the model and simulated frequency response of the designed  $50\Omega$  trace at 9.7GHz. A 51.10dB return loss is seen at 9.7GHz. The loss over a 25mm trace is 0.12dB. This verifies the model and solver are setup correctly.

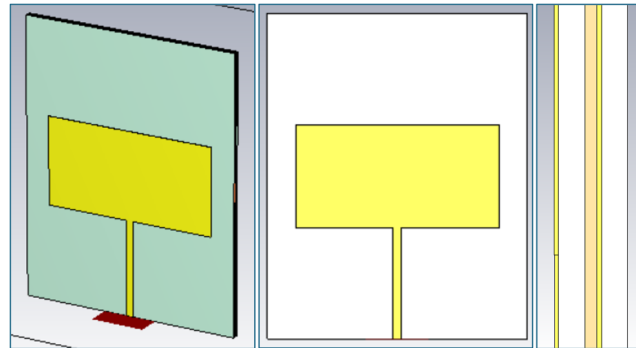


Figure 3.23: Patch antenna model in CST.

Figure 3.23 shows the initial CST Studio model used to tune the patch length and width for the designed frequency and bandwidth. Figure ? below shows the results for the initial model without any parameter tuned.

### 3.2. Antenna Detail Design

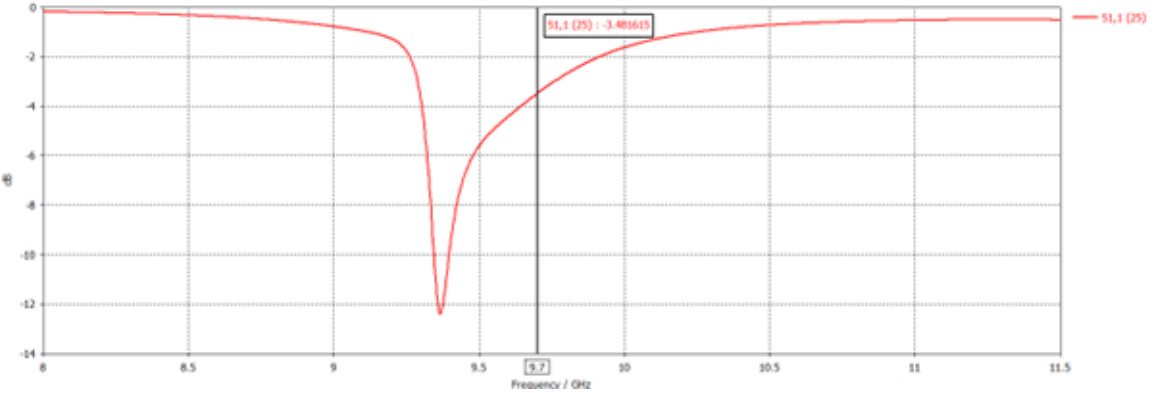


Figure 3.24: Frequency response of the patch antenna in figure 3.23.

It is observed that the center frequency is lower than the designed center frequency of 9.7GHz. The center frequency is inversely proportional to the wavelength and the wavelength is directly proportional to the dimension of the patch. Therefor the center frequency can be increased by decreasing the length of the patch, but since the width of the patch is also dependent on the length of the patch, both dimensions should slowly be decreased until the center frequency is equal to 9.7GHz. Figure 3.25 shows the return loss for the tuning of the center frequency.

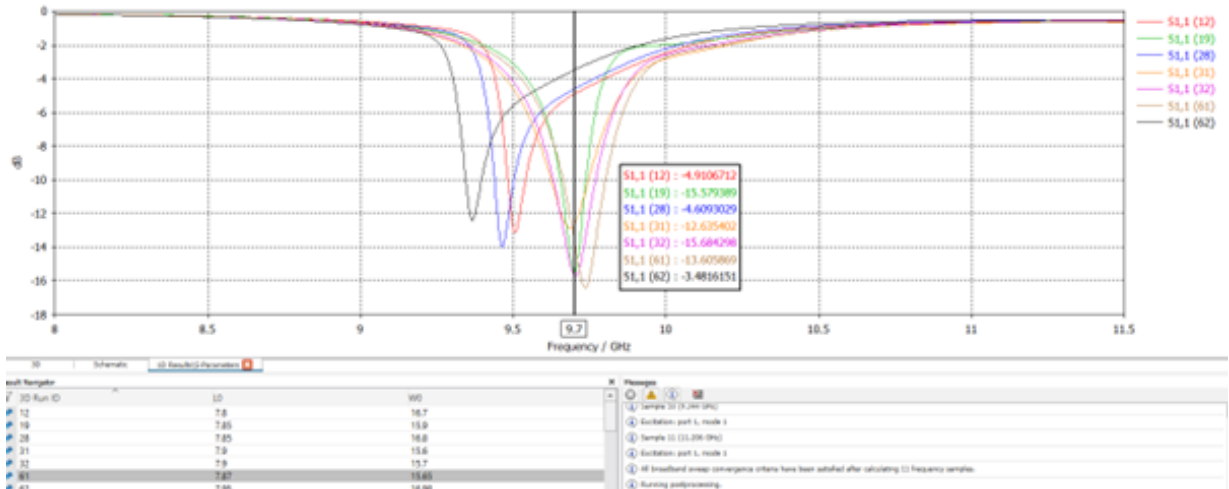


Figure 3.25: Parameter sweep results of the patch antenna in figure 3.23.

The final patch dimensions are

$$L = 7.87\text{mm}$$

$$W = 15.65\text{mm}$$

### 3.2. Antenna Detail Design

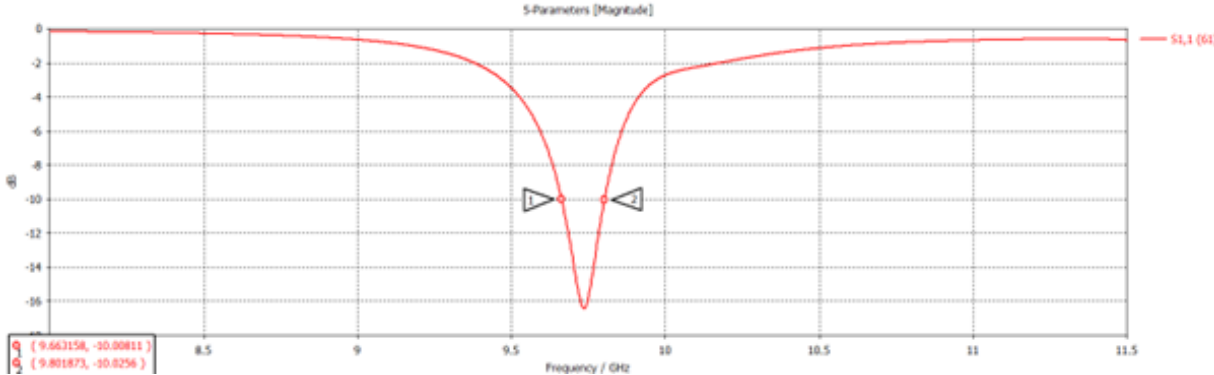


Figure 3.26: Return loss of the patch antenna before designing the feed inset.

Figure 3.26 above shows the return loss of the single patch before the feed is designed, it is seen that the  $-10\text{dB}$  bandwidth ( $B_{-10\text{dB}}$ ) is slightly lower than designed value of 150MHz. It is acceptable at this stage of the design for two reasons. Firstly, the radar bandwidth is measured from the  $-3\text{dB}$  point and the antenna bandwidth is measured from the  $-10\text{dB}$  point. Secondly the bandwidth will also change with the antenna feed design.

$$B_{-10\text{dB}} = 138.72 \text{ MHz}$$

#### 3.2.4 Feed inset

The first step to match the patch to a  $50\Omega$  system is to design a feed inset. The theoretical impedance at the edge of the patch ( $Z_A$ ) is calculated as

$$Z_A = 90 \frac{\varepsilon_r^2}{\varepsilon_r - 1} \left( \frac{L}{W} \right)^2$$

$$Z_A = 90 \frac{(3.78)^2}{(3.78) - 1} \left( \frac{7.87\text{mm}}{15.65\text{mm}} \right)^2 = 117 \Omega$$

The impedance decreases as the feed inset moves towards the center of the patch, where the impedance will be  $0\Omega$ . Since the edge impedance ( $Z_A$ ) is high then the desired  $50\Omega$ , the inset is swept from the edge to the center of the patch.

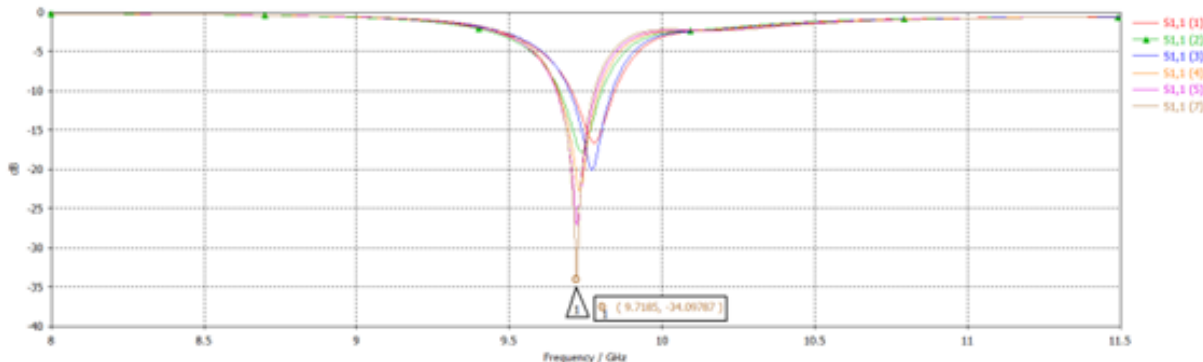


Figure 3.27: Parameter sweep results of the patch antenna's feed inset.

Figure 3.27 above shows the Return Loss of the patch as the inset is increased in steps of 0.1mm. The best performance is achieved with an inset depth of 0.6mm and the model is seen in figure 3.28 below. It is observed that the return loss improves by 17.5dB.

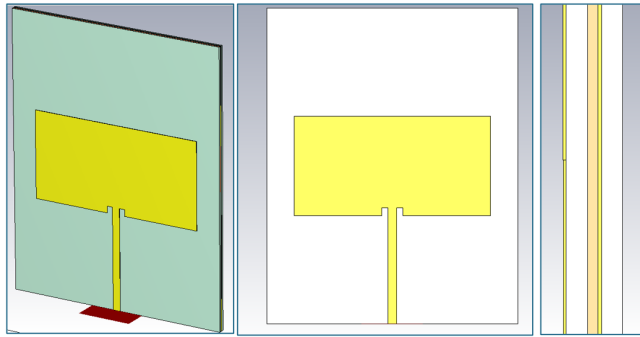


Figure 3.28: Patch antenna model after designing the feed inset.

### 3.2.5 Masking the changing of the feed

Referring to figure 3.1 in section 3 The reflected wave cannot be changed during operation, since it is determined by the physical structure of the reflector. The goal for this subsection is to minimize the phase difference caused by the reflected wave during the testing of different antennae. This allows to more accurately analyze the encoded phase of the re-radiated wave due to the changed termination of the reflector.

In the case of the reflector array the reflected wave's magnitude decreases and the absorbed wave increases if the reflector is better matched. A perfect match is not practically realizable. For the test of the antenna the feed will change frequently with either an open circuit,  $0\Omega$  resistor or connector with a SMA  $50\Omega$  load connected to the feed. Figure 3.29 below shows the possible placements for the feed termination. For figure 3.29(a) the reflected wave will change significantly as the feed termination is changed from open to short to matched. For figure 3.29(b) the feed terminations will be masked by the antenna dielectric and the ground plane layer 3, refer to figure 3.20. To achieve figure 3.29(b), an X-band via is required.

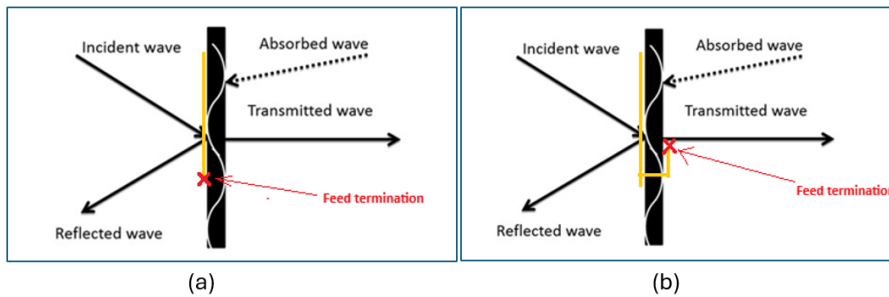


Figure 3.29: Possible placements of the terminations.

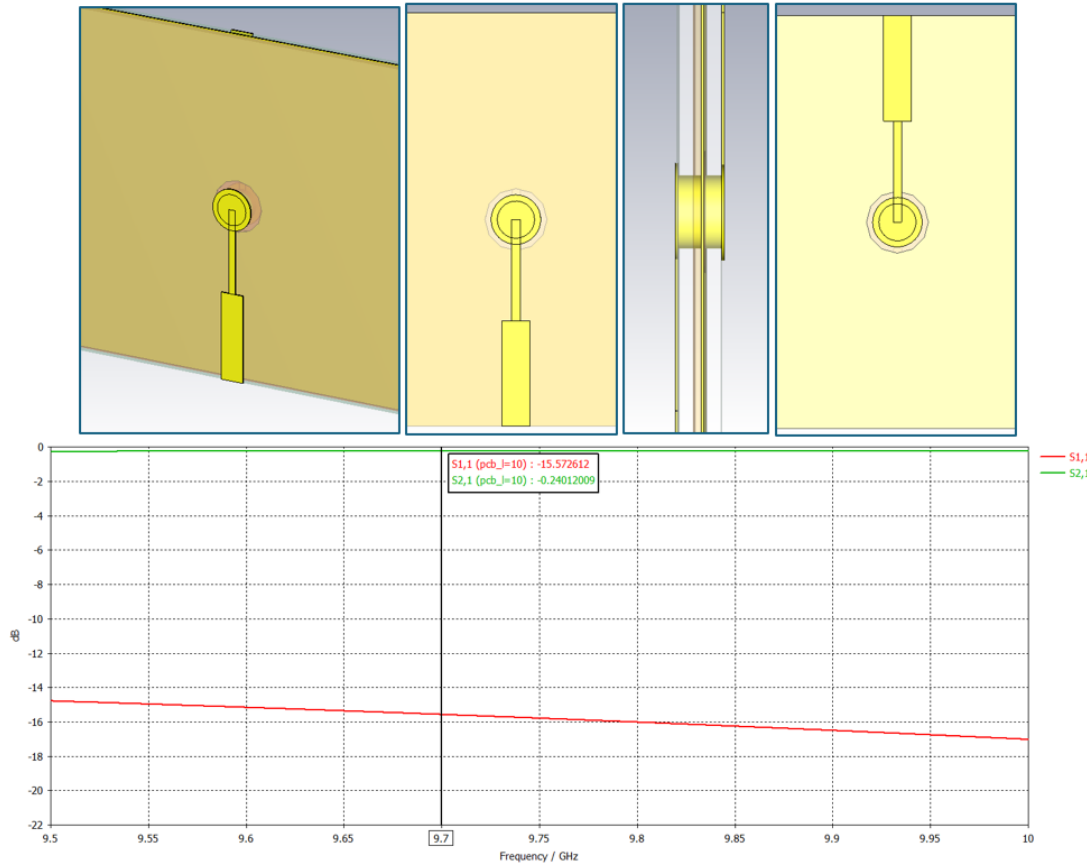


Figure 3.30: X-band via and the frequency response.

A X-band was designed previously for similar PCB stack-up. The via was simulated with the new stack-up to verify its performance. Figure 3.30 above show the via model simulated for the new stack-up along with its results. A return loss of 15.5dB and insertion loss of 0.24dB is seen at 9.7GHz. The via is added to the patch antenna. Figure 3.31 below shows the final model for a single reflector array element.

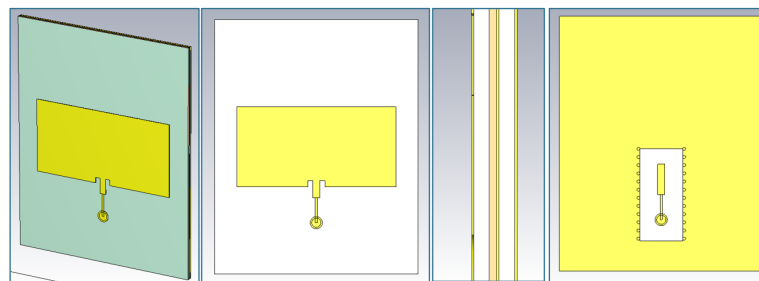


Figure 3.31: Final patch antenna model.

The bottom layer is designed to still be a microstrip trace, therefore the ground copper is pulled back more than twice the trace width. The distance between the edge of the  $50\Omega$  trace and the ground copper is equal to 1.76mm. The ground vias are blind vias to avoid changing the top layer of the antenna.

### 3.2.6 Masking the changing of the feed

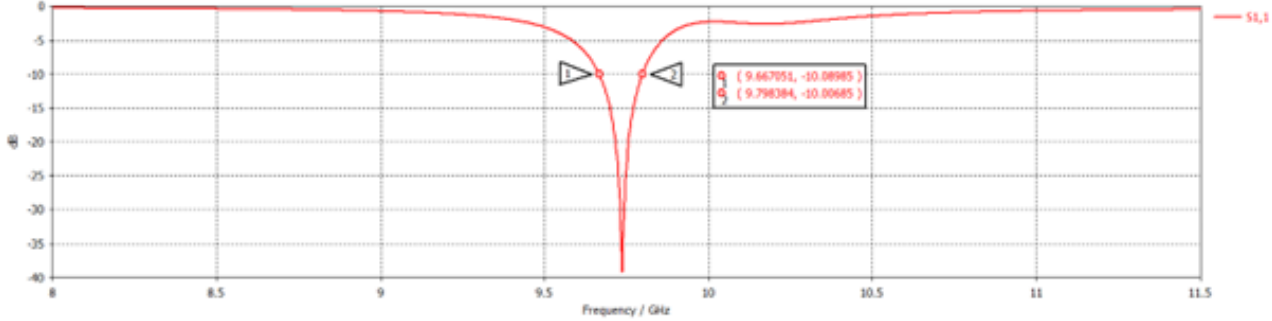


Figure 3.32: Simulated return loss of the final patch antenna in figure 3.31.

Figure 3.32 above shows the return loss of the final antenna element that will be used for the testing in this report as well as in the reflector array for future testing. Figure 3.32 show the final bandwidth ( $B_{-10dB}$ ) is a 131MHz, which is close to the design goal of 150MHz. Figure 3.33 below shows the Farfield pattern of the antenna, it is seen that the beamwidth is equal to  $75^\circ$ . The directivity is equal to 7.45dBi and no sidelobes are observed in the azimuth beam ( $\Phi=0$ ).

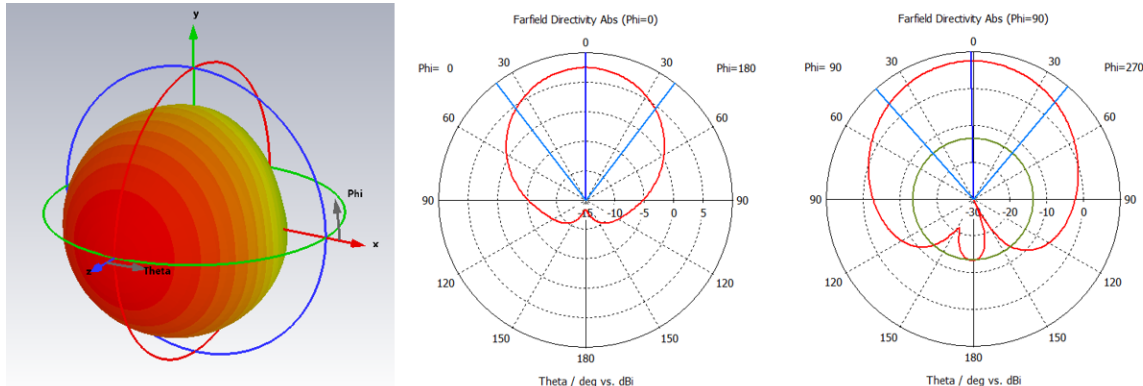


Figure 3.33: Simulated antenna pattern of the final patch antenna in figure 3.31.

Table 3.2 below summarizes the antenna parameters including the parameters needed to manufacture the antenna. The Farfield distance of the antenna is calculated below with  $D = \max(L, W)$

$$R_{ff} = \frac{2D^2}{\lambda} = \frac{2(15.65mm)^2}{30.91mm} = 15.85mm$$

Table 3.2: Dielectric comparison.

Parameter	Symbol	Value	Unit
Center Frequency	$f_0$	9.70	GHz
Wavelength	$\lambda$	30.91	mm
Dielectric Constant @ 9.7GHz	$\epsilon_r$	3.78	-
Substrate thickness	$t$	0.31	mm
Patch length	$L$	7.87	mm
Bandwidth	$B_{-10dB}$	131.33	MHz
Patch width	$W$	15.65	mm
Patch ground length	$L_g$	25.00	mm
Patch ground width	$W_g$	20.00	mm
copper thickness	$t_{cu}$	35.00	um
50 Ohm trace width	$W_{50\Omega}$	0.68	mm
Feed inset	$\Delta x_p$	0.60	mm
Feed gap	$\Delta g_p$	0.50	mm
Via hole diameter	$d_i$	0.90	mm
Via pad external pad diameter	$d_p$	0.60	mm
Via ground pull back	$d_o$	1.50	mm
Via matching strip width	$W_{strip}$	0.20	mm
Via matching strip length measured from the center of the via	$L_{strip}$	2.45	mm

### 3.2.7 Linear & 2D reflector array design

PCB manufacturers quote per dielectric sheet. Since a single element is only 25x20mm and this investigation only requires 3 antennas, a 1x4 and a 4x4 reflector were also designed for future testing and manufactured alongside the single elements.

Since the beam will not be steered the antenna spacing is not limited by a grating lobe requirement. This means the antennas can be spaced more than half a wavelength ( $\frac{\lambda}{2}$ ). The antennas are space 20mm apart. This allows 4.35mm between the adjacent edges of the array elements. Figure 3.34 below shows the CST model along with the simulated coupling.

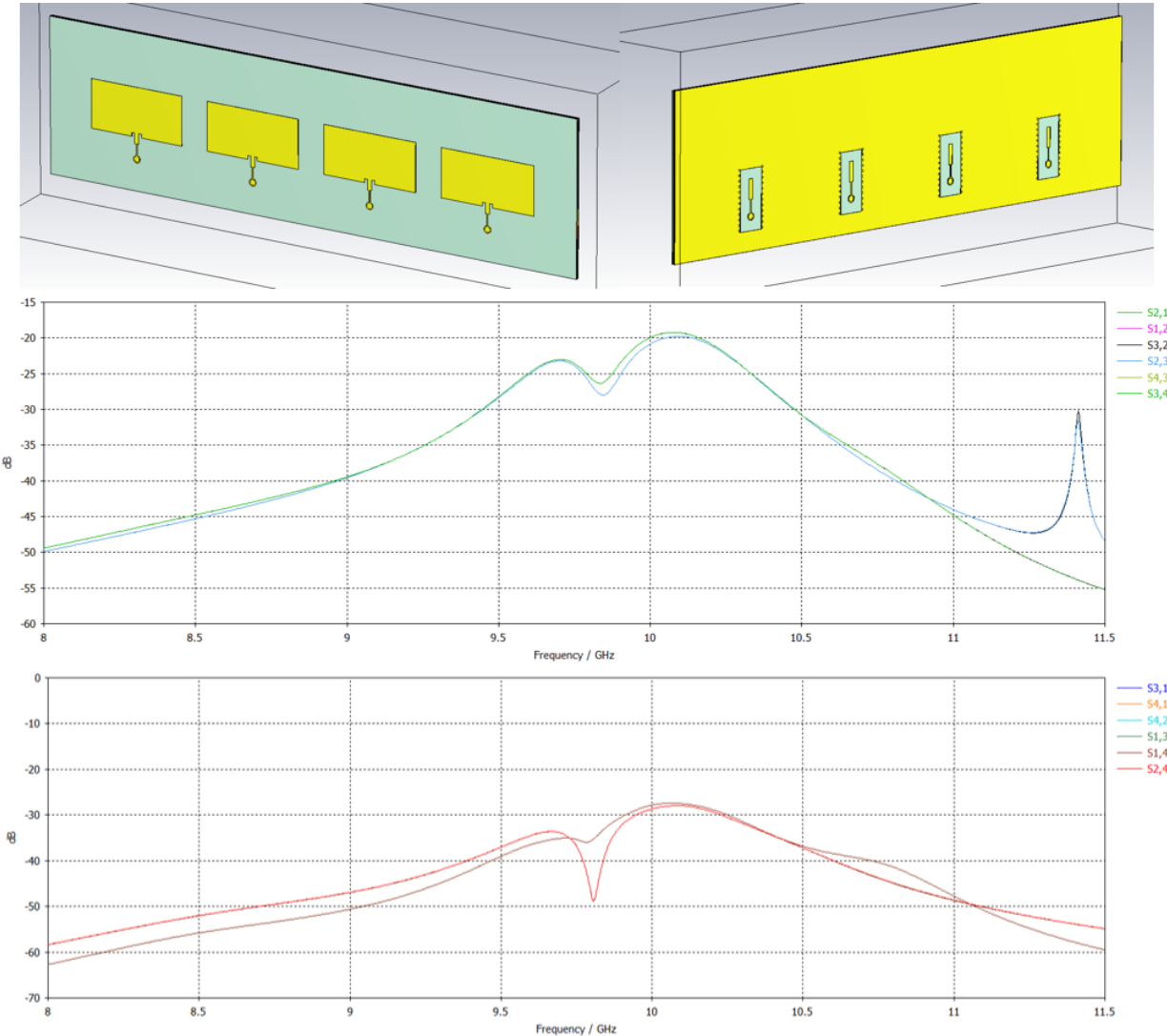


Figure 3.34: Linear patch array and simulated coupling.

Figure 3.34 graph shows the coupling from the adjacent array elements (top) and the coupling from every second element as well as the coupling between the edge elements (bottom). Figure ? below shows the return loss of all the elements. No variation is observed and the spacing is far enough that the coupling does not affect the antenna performance. The Farfield pattern is the Array Pattern (AP) times the Element Pattern (EP). Figure 3.35 below shows the Farfield pattern of the linear array, it is seen the beamwidth is equal to  $19.5^\circ$ . This is significantly lower than the  $75^\circ$  of a single element due to the array pattern having a narrow beamwidth. The gain of the array is equal to 13.17dBi, which is a 5.72dB improvement from the single element. A Sidelobe level (SLL) of -13.2dBc or -0.03dBi is observed.

$$AP * EP = \text{Farfield Pattern}$$

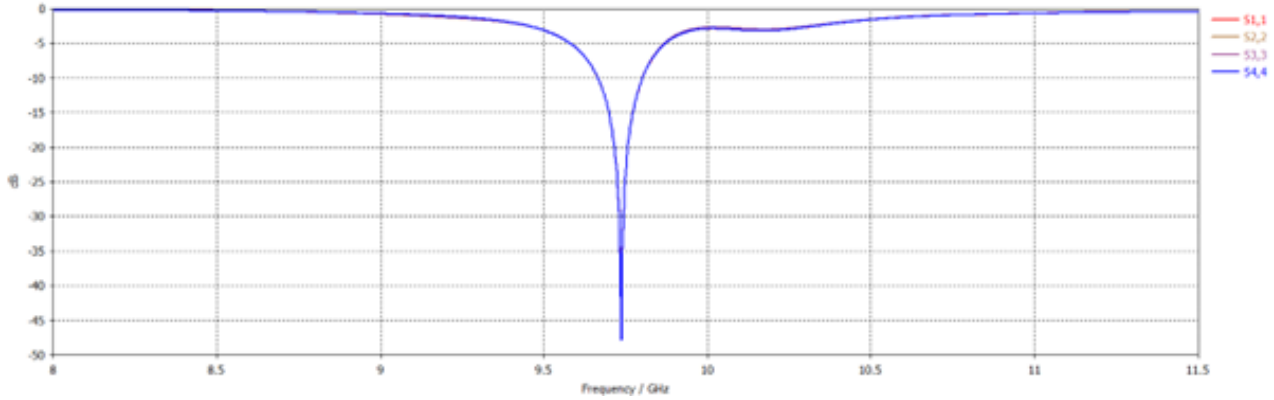


Figure 3.35: Simulated return loss of the linear patch array.

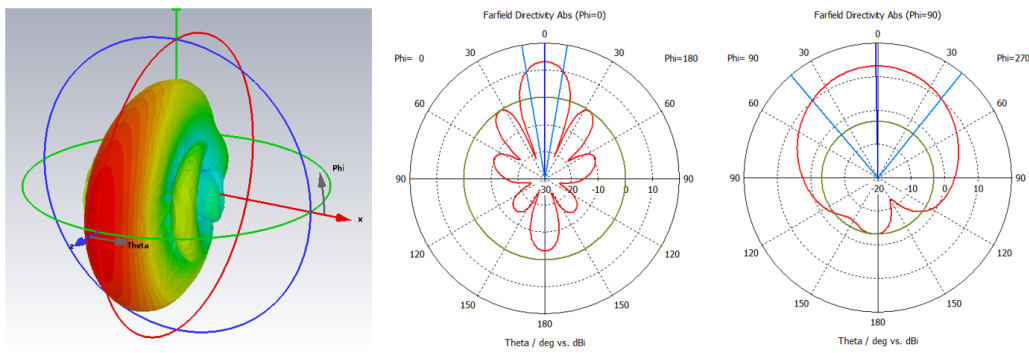


Figure 3.36: Simulated farfield pattern of the linear patch array.

The linear array was adapted to a 2-dimensional reflector array with the vertical antenna spacing also equal to 20mm. This allows 8mm between the top edge of the array elements and the edge of the via pad. Figure 3.37 below shows the CST model along with the simulated coupling.

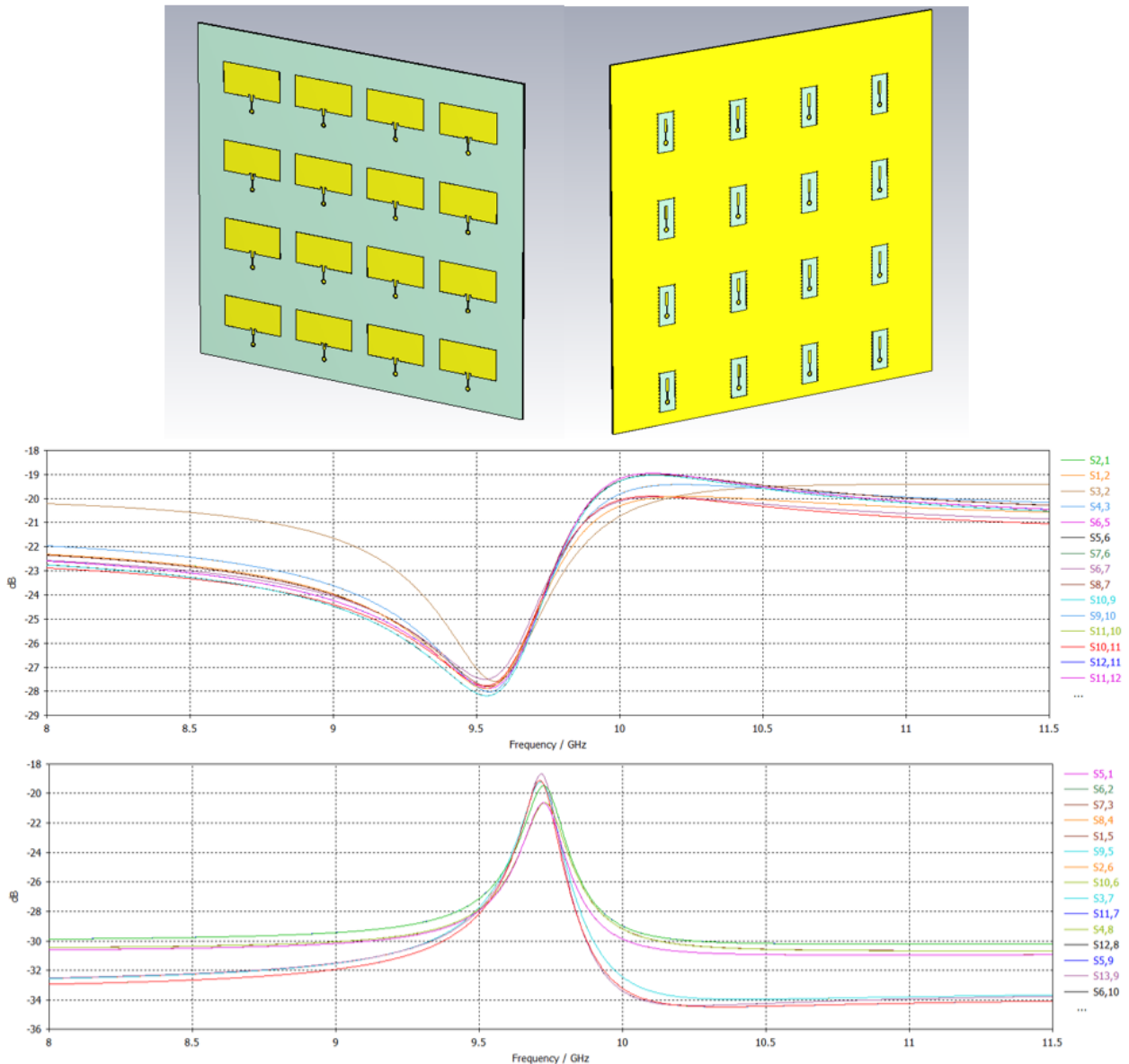


Figure 3.37: 2D patch array and simulated coupling.

Figure 3.37 shows the coupling from the horizontally adjacent array elements (top) and the coupling from the vertically adjacent array elements (bottom). Figure 3.38 below shows the return loss of all the elements. No variation is observed and the spacing is far enough that the coupling does not affect the antenna performance. Figure 3.39 below shows the Farfield pattern of the 2-dimensional array, it is seen the beamwidth is equal to  $19.4^\circ$ . The gain of the array is equal to 13.14dBi, which very similar to the linear array. The sidelobe level (SLL) of -14.3dBc or -0.26dBi is observed, which is a 1dB improvement over the linear array.

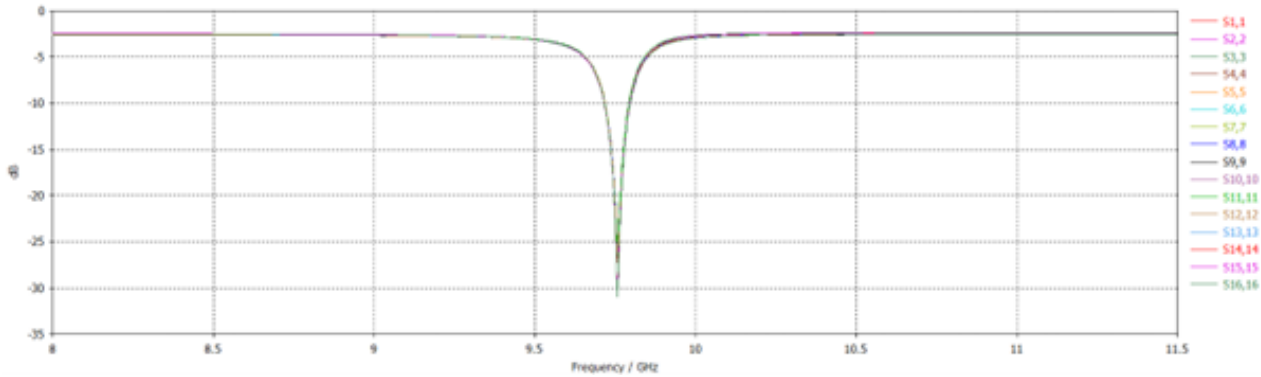


Figure 3.38: Simulated return loss of the 2D patch array.

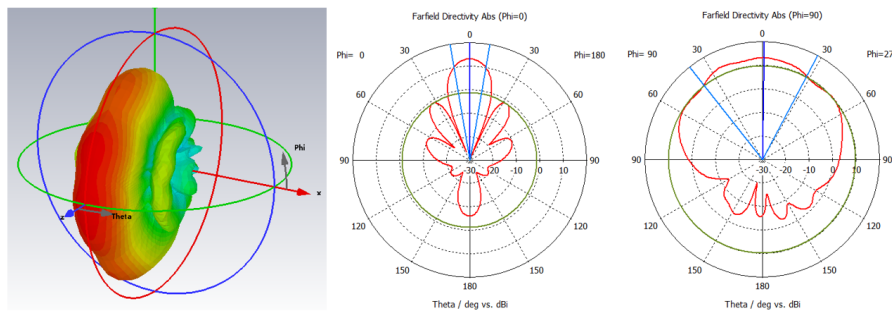


Figure 3.39: Simulated farfield pattern of the 2D patch array.

### 3.2.8 Manufacturing

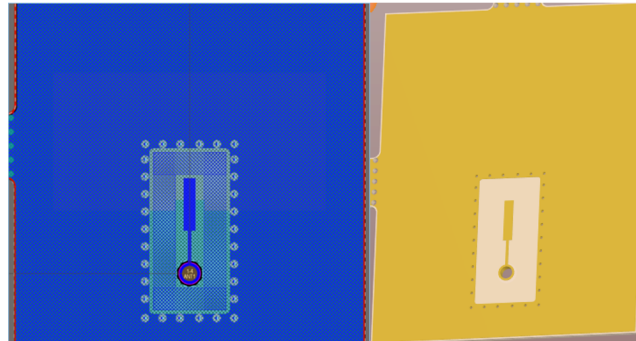


Figure 3.40: Single patch antenna in Altium.

To be able to measure the response of the antenna, a connector is required. Figure 3.41 below shows the Altium 2D and 3D view of the surface mount SMP connector used. Since the interest is focussed on the open and short circuit termination the effort of designing the RF transition was not done, the manufacturers recommended footprint up to 18GHz is used.

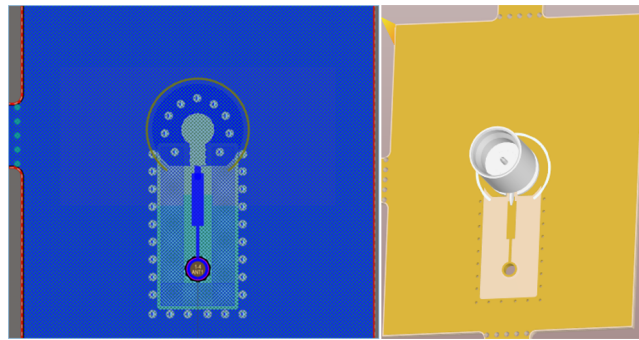


Figure 3.41: Single patch antenna with a SMP connector in Altium.

Maximizing the use of the dielectric sheet size as specified by the PCB manufacturer results in the final PCB seen in figure 3.42 below. Four single antenna elements are manufactured, two of which as a SMP connector on the feed. One of the two single elements without a connector will remain an open circuit, whilst the other element will be shorted with a  $0\Omega$  resistor.

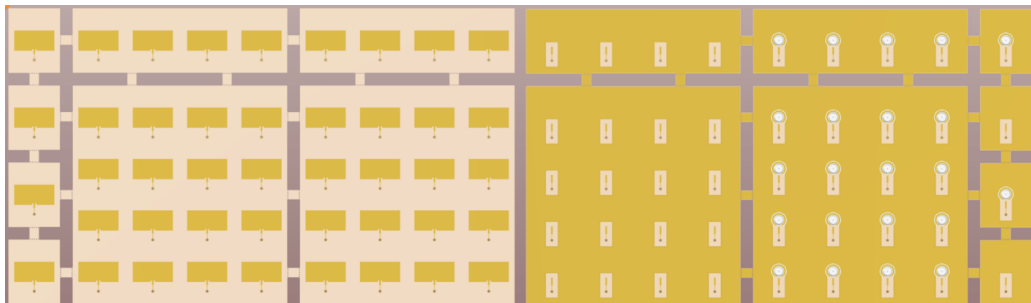


Figure 3.42: Manufactured Altium PCB.

The manufactured antenna has a visible warp and due to this a mounting solution is required that will pull the antenna flat again. The warping is due to the very thin PCB thickness of 624um and the removed copper on layer 2 creating an asymmetrical stack-up. A better antenna design would include mounting hole to screw the antenna to a plate or bracket.



Figure 3.43: Manufactured patch array with visible warping.

The quickest solution available due to the lack of mounting holes was a 3D printed bracket. The first solution below securely held the antenna in place with no visible flexing or cracking.

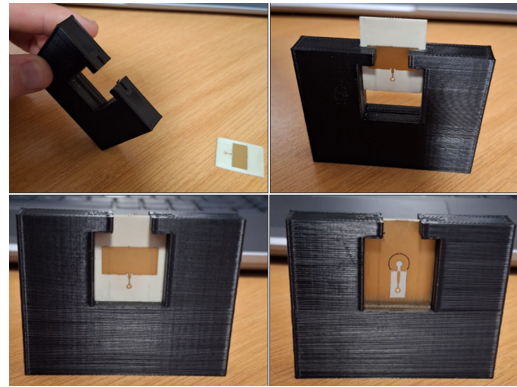


Figure 3.44: First iteration of the mounting bracket.

However, the bracket was not high enough to easily align the three antennae using during testing. Also, due to the wide beamwidth of a single element patch antenna there was still a concern the  $90^\circ$  edges left and right of the antenna are seen by the beam.

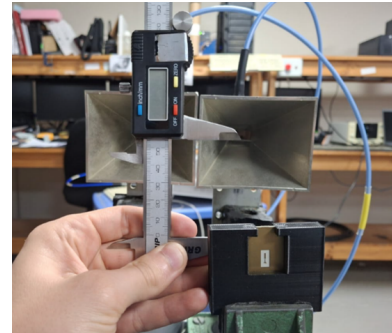


Figure 3.45: Height misalignment of the first bracket.

The second version solve both issues by increasing the height of the bracket as well as adding  $45^\circ$  chamfers to the front face of the bracket.

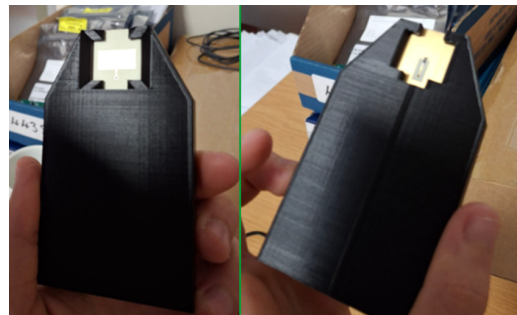


Figure 3.46: First iteration of the mounting bracket.

### 3.3 Measurement Processing

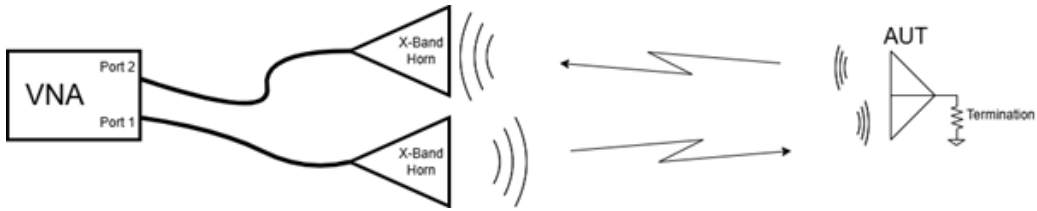


Figure 3.47: Block diagram of the required test setup.

Figure 3.47 shows the planned test setup. A two port Vector Network Analyzer (VNA) is required to be able to measure the phase of the received reflected signals from the Antenna Under Test (AUT). Unfortunately the VNA will measure more than just the re-radiated signal from the reflector and the measured  $S_{21}$  parameter will need to be processed to isolate the phase encoded signal.

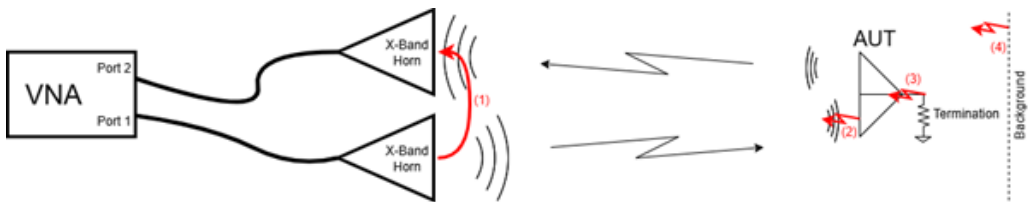


Figure 3.48: Reflections measured by the receiver horn antenna.

Referring to figure 3.48 above, the received signal at port 2 will be the superposition of the following:

1. The coupled signal from transmitter X-Band horn antenna.
2. The reflected signal from the antenna, refer to figure 3.1 in section 3.
3. The re-radiated signal, which will be encoded with a phase.
4. The reflected signals from the surrounding background.

For the proposed system in section 1.3 to be realizable, the effect of signals (1), (2) and (4) needs to be able to be calibrated out of the received signal at port 2. The same applies to the tests required for this investigation. To solve this a  $50\Omega$  load is connected to the antenna for a separate matched measurement. The assumption is that if all of the absorbed wave from the AUT is also absorbed by the matched load connected to the antenna, then the signal measured at port 2 will only consist of signals (1), (2) and (4). Therefore, if the  $S_{21}$  of the matched measurement is subtracted from the  $S_{21}$  at of the open and short circuit measurement, the only remaining signal is (2), the re-radiated signal, which will be encoded with a phase.

The processing chain to achieve this is described in this section. The processing chain is written in MATLAB after saving the touchstone files from the VNA. The script opens and reads only the  $S_{21}$  from the required touchstone files. The  $S_{21}$  of the matched, open and short circuit measurement are plotted on a smith chart at the center frequency of 9.7GHz. The matched  $S_{21}$  is then subtracted from the open and short circuit measurement and plotted again to verify.

```
%%%%%% IMPORT MEASUREMENTS %%%%%%
match      = sparameters('900mm/Match_900mm_20250429.s2p');
open       = sparameters('900mm/Open_900mm_20250429.s2p');
short      = sparameters('900mm/Short_900mm_20250429.s2p');
matchs21_900 = rfparam(match,2,1);
opens21_900 = rfparam(open,2,1);
shorts21_900 = rfparam(short,2,1);
freq = short.Frequencies/1e9;
fmin = 9;
fmax = 10;
kmin = find(freq>fmin, 1, "first");
kmax = find(freq<fmax, 1, "last");

%%%%%%%%% NORMALIZE ALL MEASUREMENTS TO MATCH LOAD %%%%%%
opens21_900 = opens21_900-matchs21_900;
shorts21_900 = shorts21_900-matchs21_900;
matchs21_900 = matchs21_900-matchs21_900;
```

Figure 3.49: MATLAB script to import and normalize the  $S_{21}$  to the  $50\Omega S_{21}$ .

As stated in section 2.4 the signal at a short circuit will be reflected with a  $180^\circ$  phase change, but the signal at an open circuit will be reflected with no phase change. Therefore, the theoretical phase between the open and the short circuit measurement after subtracting the matched measurement should be a fixed  $180^\circ$  difference. The script therefore subtracts the phase of the short circuit measurement from the open circuit measurement and plots the results over frequency. All the samples in the bandwidth of the antenna is then used to calculate the mean and the standard deviation of phase difference. The error is then measured from the mean for all measurements that were imported.

```
%%%%% DIFFERENCE BETWEEN OPEN & SHORT %%%%%%
diff_900    = rad2deg(angle(opens21_900)-angle(shorts21_900));

%%%%%%%% 150MHz Bandwidth around 9.5GHz %%%%%%
freq = short.Frequencies/1e9;
fmin = 9.425;
fmax = 9.575;
kmin = find(freq>fmin, 1, "first");
kmax = find(freq<fmax, 1, "last");

%%%%%%%% MEAN & STD %%%%%%
all_data    = [diff_900(kmin:kmax)];
std_all_freq = std(all_data);
all_data    = all_data';
mean_all    = mean(all_data);
mean_all_avg = mean(mean_all);
std_all     = std(all_data);
std_all_avg = mean(std_all);
rms_all     = rms(all_data);
all_data_f  = fit(freq(kmin:kmax), mean_all', 'poly2');
fit_all_data = feval(all_data_f, freq(kmin:kmax));

%%%%%%%% RMS ERROR %%%%%%
rmse_900    = rmse(mean_all', diff_900(kmin:kmax));
error_900    = diff_900(kmin:kmax)-mean_all';
error_all_data = [error_900];
```

Figure 3.50: MATLAB script to analyze the encoded phase and the error of the AUT.

It is crucial to only subtract the phases of each  $S_{21}$  and not the complex values. If the complex value is subtracted first then the resulting phase would be  $\Phi$  in figure 3.51 below and not  $\Theta$ .

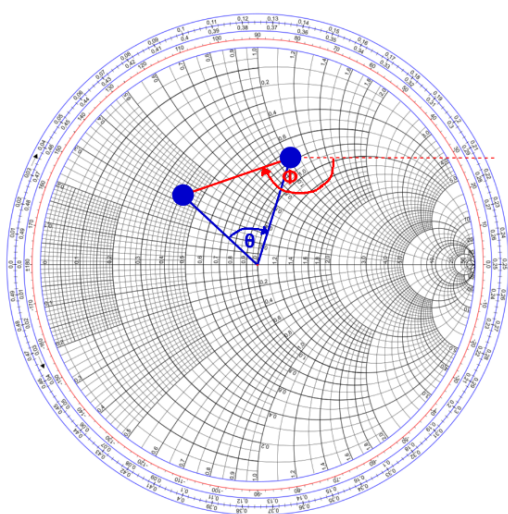


Figure 3.51: Smith chart with phase relative phase angles.

# Chapter 4

## Testing & Results

### 4.1 Test setup & Equipment

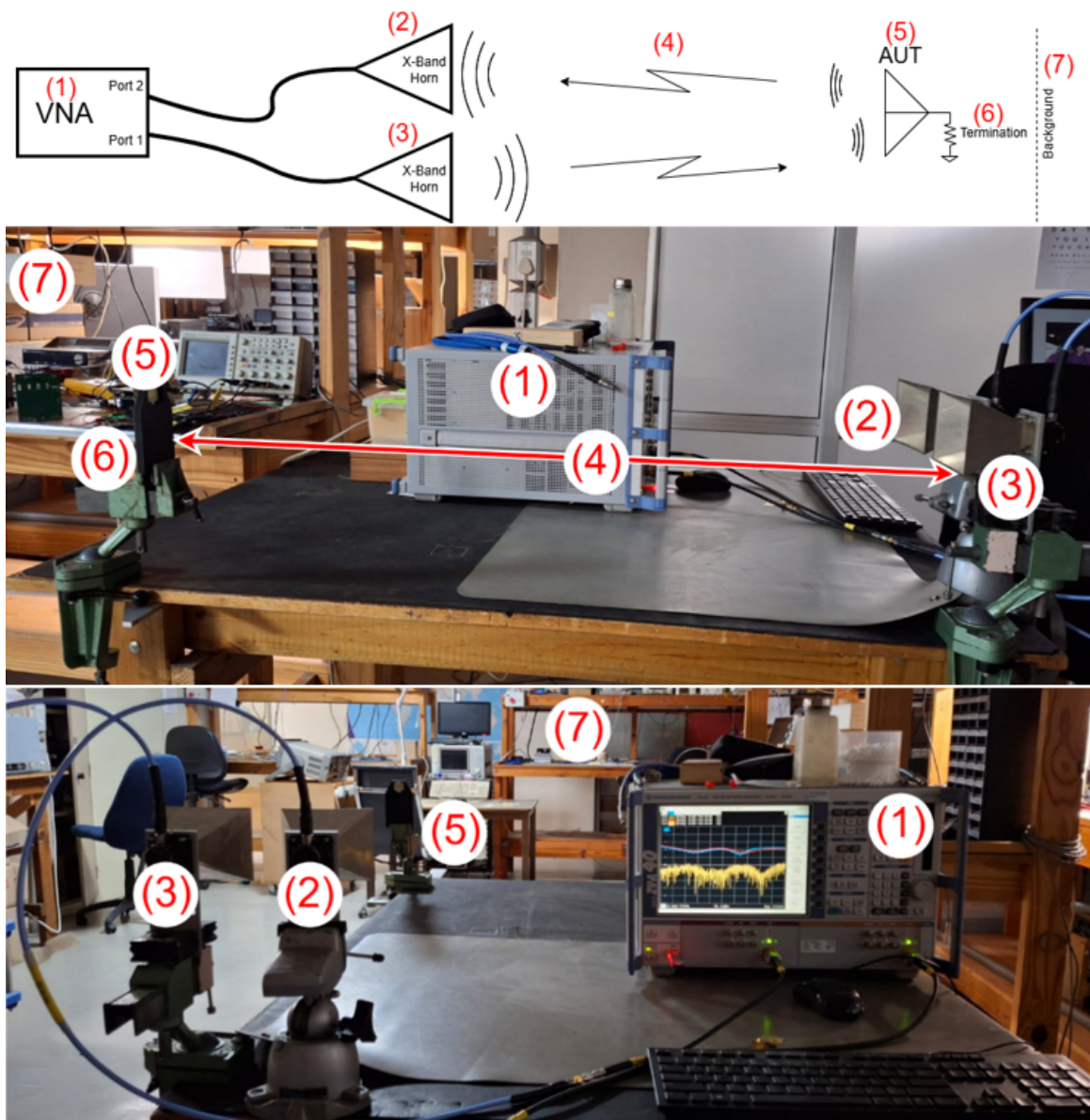


Figure 4.1: Test Setup.

#### 4.1. Test setup & Equipment

Figure 4.1 show the labelled block diagram of the test setup along with the labelled physical test setup used for all the measurements in this section.

1. The Rohde & Schwarz ZVA 40 VNA was used. This a 2 port  $10MHz - 40GHz$  VNA.
2. This is one of two identical reflective covered injection moulded X-band horn antennae. This antenna acts as the transmit antenna. Since the signal measured will be extremely small in magnitude a horn antenna was chosen for the high gain and directivity.
3. This is the other X-band horn antennae that was used as the receive antenna. The center of the aperture of the horn antennae are aligned.
4. The AUT must be placed in the Farfield region of all the antennae. Since the X-Band horn antenna have the largest aperture, the min distance will be the were the Farfield of the horn antennae start.
5. The AUT is placed in the design bracket and the bracket does not move for a set of measurements. The bracket is designed to keep the position of the AUT fixed when swapping the antennae. The center of the patch is aligned with the aperture of the horn antennae.
6. Instead of changing the termination of each measurement, three different antennae are used with a termination connect. See figure 4.2 below.
7. Since the measurement were done in the laboratory of a Radar company, the measurements were done after hours and all other equipment in the laboratory was switched off.



Figure 4.2: Three different AUT used during testing.

Before the investigation can be done with the design patch antenna, the antenna design must first be verified. The measured return loss of the connectorized antenna is seen in figure 4.3 below. Although the deep null of -40dB is not seen, the return loss of -19.5dB at the center frequency is still a well-designed antenna. The center frequency is also lower by a 98MHz which equates to a difference in antenna width of  $\pm 200\mu m$  or antenna length of  $\pm 90\mu m$  according to CST studio simulations.

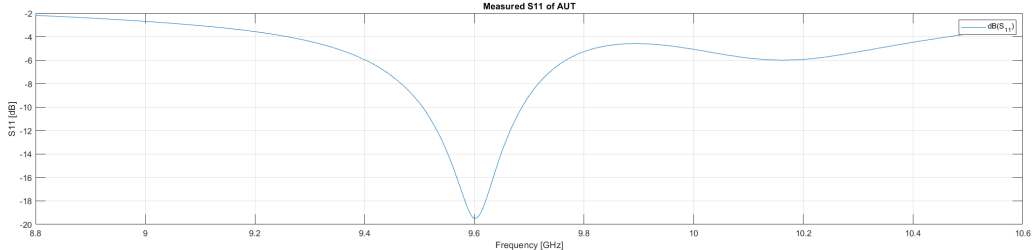


Figure 4.3: Measured return loss of the design patch (AUT).

## 4.2 Results

The test procedure involves moving the AUT into the Farfield of the X-Band horn antennae then doing three separate measurements. One with the open load antenna, a second with the short-circuited antenna a third with the SMP antenna with a SMA  $50\Omega$  termination connected to it. The Farfield region of the X-Band horn is calculated below as 584mm. At set of measurements were done with the AUT 600mm, 700mm, 800mm and 900mm away from the horn antennae.

$$R_{ff} = \frac{2D^2}{\lambda} = \frac{2(95\text{mm})^2}{30.91\text{mm}} = 584\text{mm}$$

Analyzing the raw  $S_{21}$  data for the 800mm measurements, as seen in figure 4.4 below, the measured magnitude is the same for both the short circuit and the open circuit AUT. The only visible difference is near the center frequency of the AUT. The same is seen in figure 4.4 for the measured  $S_{21}$  phases of the short circuit and open circuit AUT.

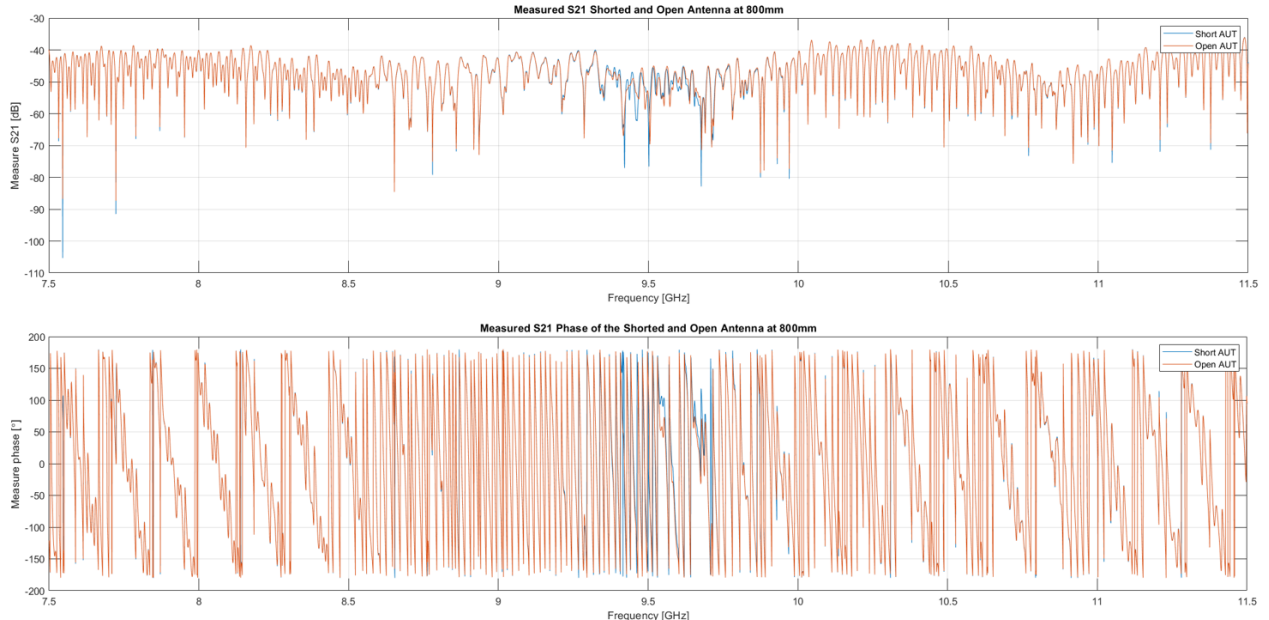


Figure 4.4: Measured  $S_{21}$  magnitude & phase.

Figure 4.5 below show the zoomed-in view of figure 4.4 as well as the phase difference between the

## 4.2. Results

short circuit and open circuit AUT of the measured and unprocessed  $S_{21}$ . It is clear that the maximum difference occurs close to the center frequency, which is the opposite response that is aimed for. The following section details the results of the signal processing required for the proposed system in section 1.3.

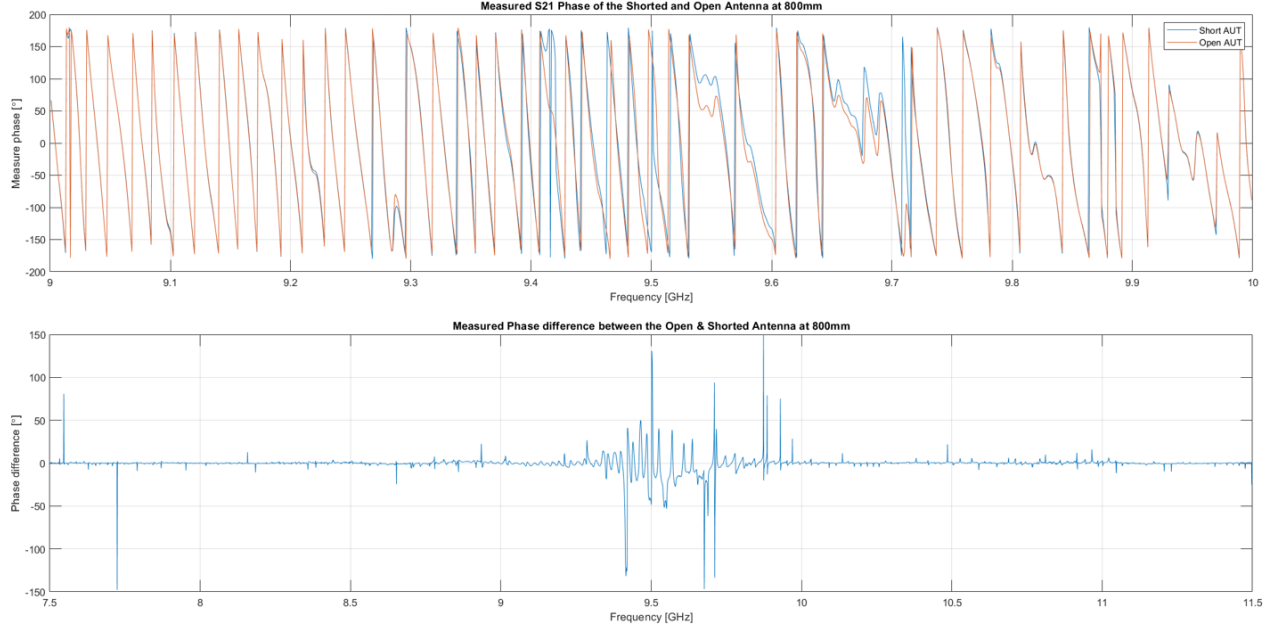


Figure 4.5: Measured and unprocessed phase difference between the open and short AUT.

Figure 4.6 below shows the  $S_{21}$  at the center frequency plotted on the smith chart. Since the power loss from the transmit horn antenna through the test setup to the receive antenna is high, the magnitude of the  $S_{21}$  is very low. Due to this all three  $S_{21}$  points are difficult to see, figure 4.6 (bottom) shows the same plot with a scale of 0.0032.

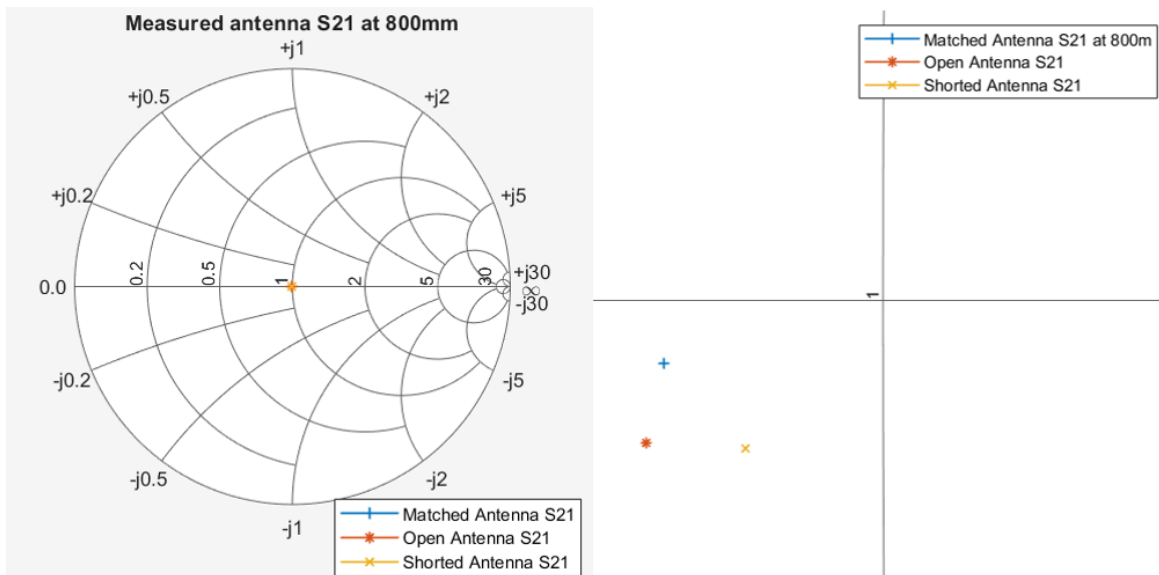


Figure 4.6: Measured and unprocessed  $S_{21}$  plotted on the smith chart.

For the proposed system in section 1.3, it is assumed that the background and physical AUT remains constant for a given measurement. If that this assumption holds true, then the reflections received from the scene will be the same in the short circuit and open circuit measurement. Therefor this can be calibrated out. For the testing in this report the matched AUT should absorb all the received power into the  $50\Omega$  load and the received signal should only contain the reflections from the background and the physical structure of the AUT. Therefor all the measured  $S_{21}$  data is normalized to the matched  $S_{21}$  data as seen in figure 4.7 below.

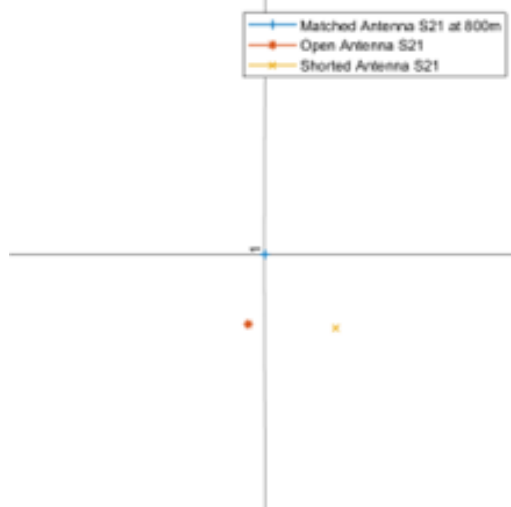


Figure 4.7:  $S_{21}$  normalized to the  $50\Omega S_{21}$  plotted on the smith chart.

Now that the short circuit and open circuit  $S_{21}$  has been normalized, the phase difference can be recalculated. Figure 4.8 below shows the result over the entire measured frequency span. The spikes observed are due to the phase wrapping. Figure 4.8(bottom) show the result over the over the entire measured frequency span with the unwrapped phase.

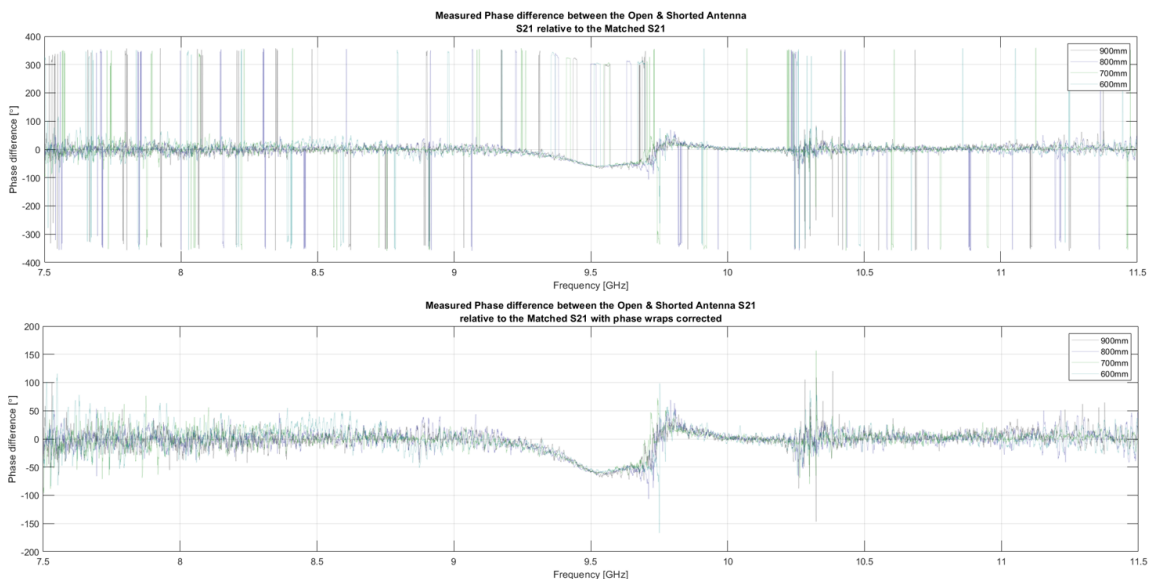


Figure 4.8: Encoded phase difference of the AUT normalized to the  $50\Omega S_{21}$ .

## 4.2. Results

It is undeniable that the phase difference becomes smaller the closer the measurement is to the center frequency. Figure 4.9 below shows a zoomed-in plot of the phase difference. Using the antenna parameters as a guide the error calculations are done from 9.425-9.575GHz.

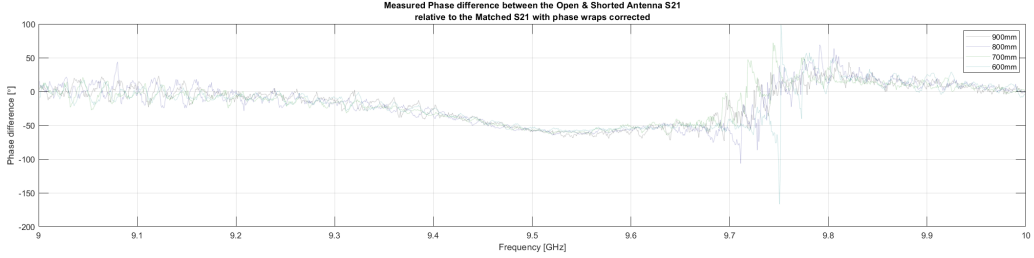


Figure 4.9: Zoomed-in plot of figure 4.8(bottom).

Figure 4.10(top) shows the mean of the four measurement sets over frequency along with the standard deviation from the mean over frequency (middle). The average of the mean is calculated as  $-53.71^\circ$  and the average standard deviation is calculated as  $2.66^\circ$ . The phase error for each data set is seen in figure 4.10(bottom). The RMS phase error for each data set is noted in table 4.1. These are very promising results, however the sample size is small and all four measurements set were recorded on the same day with the same environment.

Table 4.1: Phase error of first set of measurements

Data set	RMS error [°]
900mm	2.7193
800mm	2.7260
700mm	1.4218
600mm	2.9145

## 4.2. Results

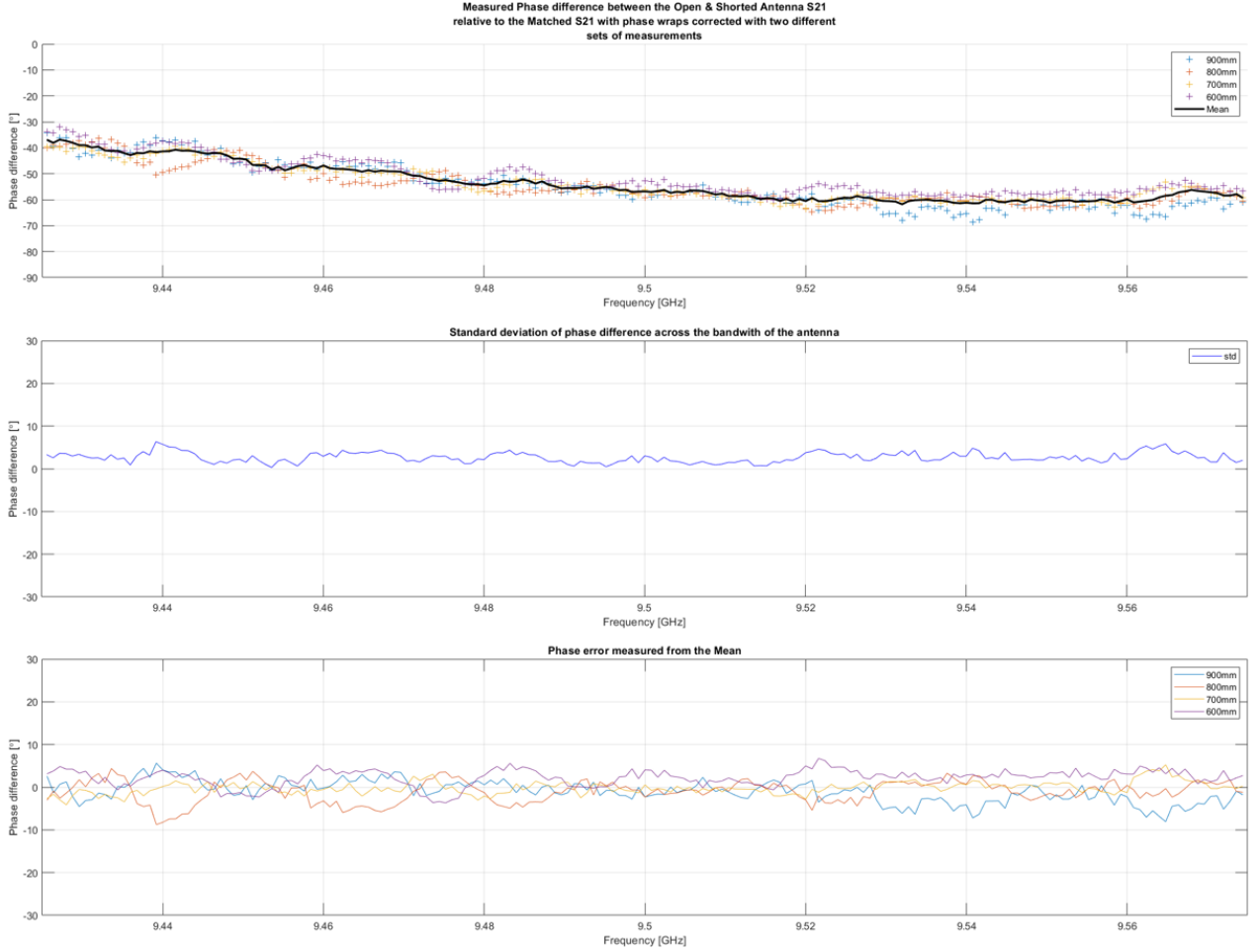


Figure 4.10: Mean, standard deviation and phase error of first set of measurements.

The tests are repeated two weeks after the original testing was completed to confirm that the results are correct and repeatable. Figure 4.11(left) is from the first day of testing, figure 4.11(right) is from the second day of testing. It is seen that the figure after normalizing to the  $50\Omega S_{21}$  the second measurement looks like a rotated version of the first measurement. The visual inspection is promising.

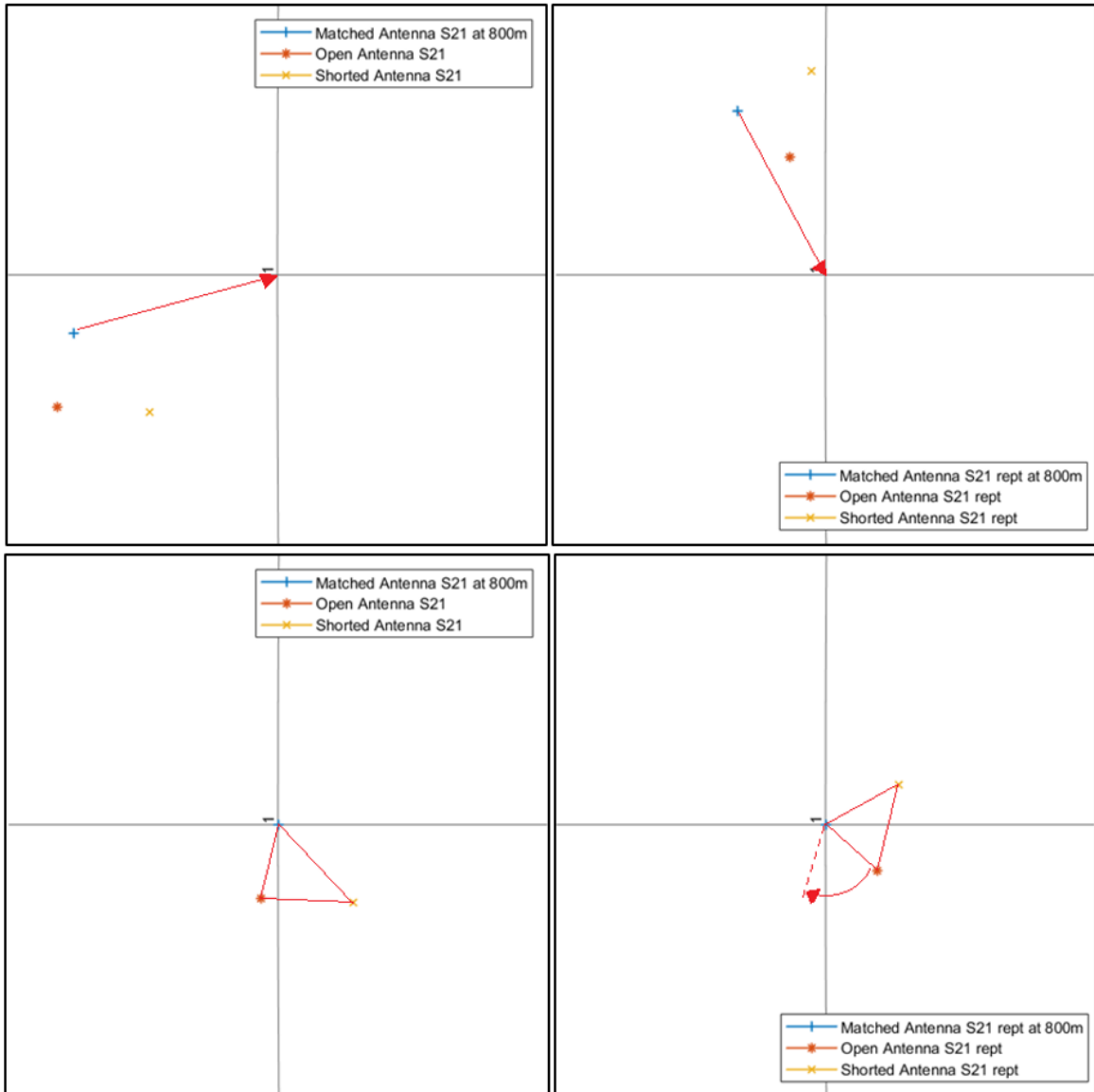


Figure 4.11: First set  $S_{21}$  (left), Second set  $S_{21}$  (right).

Figure 4.12 below shows the encoded phase difference between the short circuit and open circuit after being normalized to the matched  $S_{21}$ . Figure 4.12(bottom) shows the same data overlayed over the first day of testing's results. The response is similar, but slightly more sporadic.

## 4.2. Results

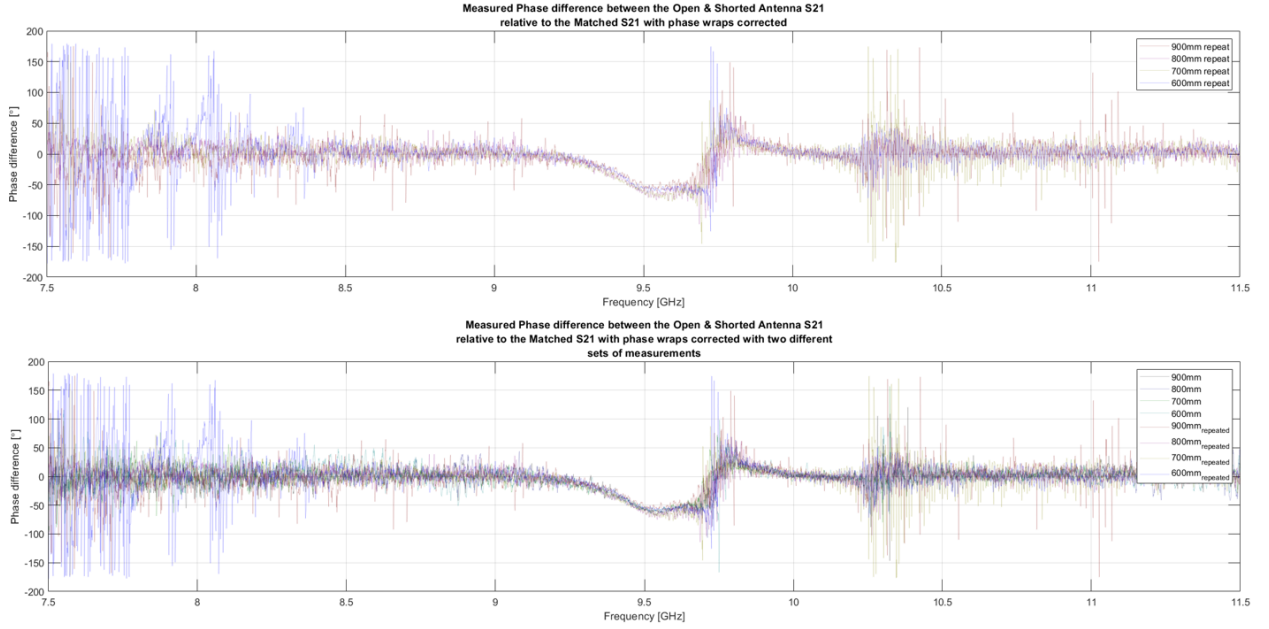


Figure 4.12: Encoded phase difference of the AUT normalized to the  $50\Omega S_{21}$ .

Figure 4.13(top) shows the recalculated mean of all the measurement sets along with the recalculated and the original standard deviation from the mean (middle). The average of the mean is calculated as  $-54.06^\circ$ , which is within  $0.4^\circ$  of the original mean. The average standard deviation is calculated as  $4.19^\circ$ , which has increased by  $1.5^\circ$  from the original standard deviation. The phase error for each data set is seen in figure 4.13(bottom). The RMS phase error for each data set is noted in table 4.2 and a clear increase is observed.

Table 4.2: Phase error of all measurements

Data set	RMS error for day 1 [°]	RMS error for day 2 [°]
900mm	2.7193	6.1314
800mm	2.7260	5.0576
700mm	1.4218	5.2886
600mm	2.9145	3.1176

## 4.2. Results

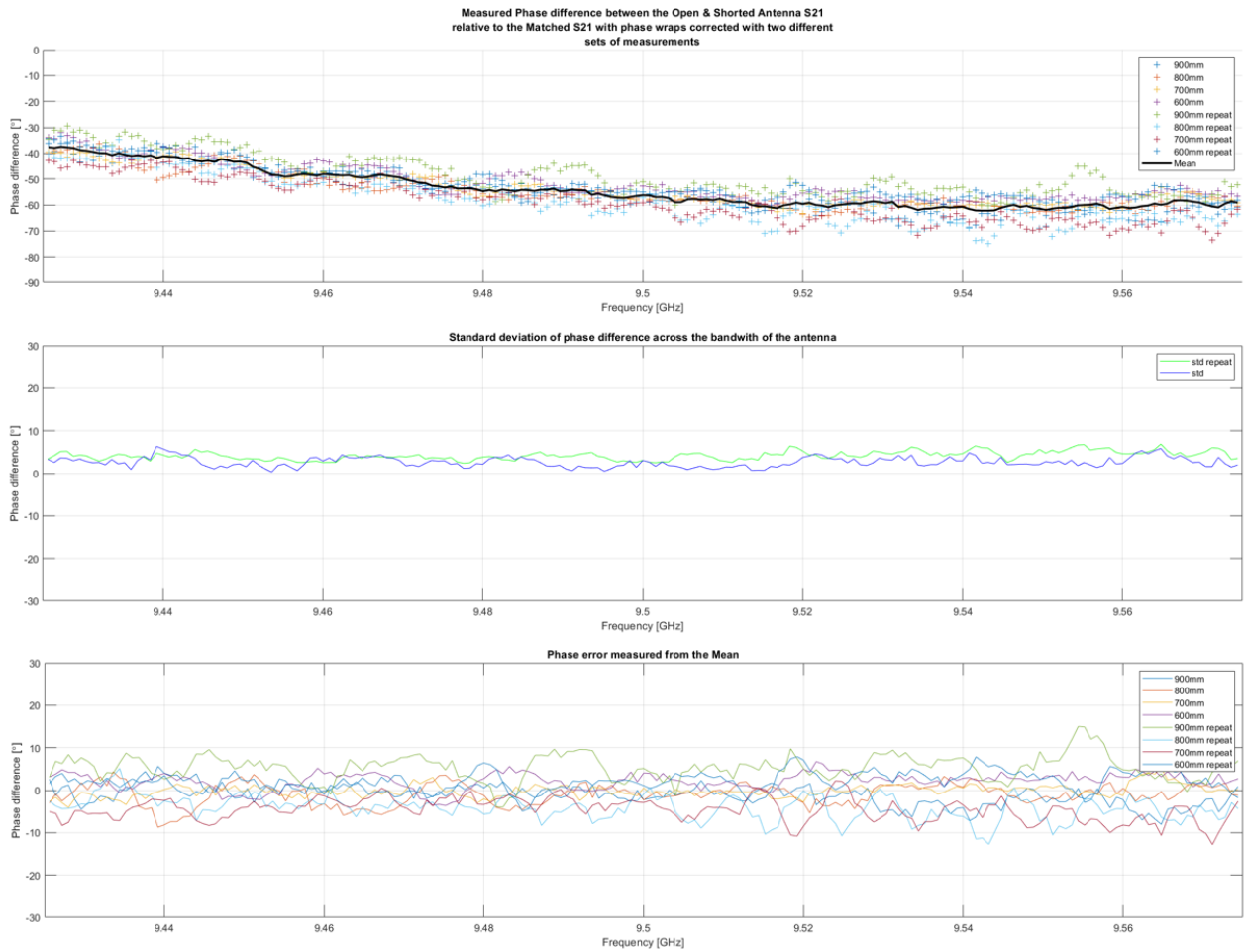


Figure 4.13: Mean, standard deviation and phase error of all measurements.

# Chapter 5

## Conclusions

The results verify the hypothesis. The results prove that a phase difference can be encoded by merely changing the reflector antenna's load from an open to a short circuit, however the phase difference that is encoded is not equal to the theorized  $180^\circ$ . The phase difference that is encoded is only  $54^\circ$ . This could be due to the path length of the reflectors feed. A possible test would be to use a through hole feed to move the termination closer to the antenna's surface.

The RMS error can be quite large at  $6^\circ$  for the second set of measurements. A possible way to improve this is to repeat the tests with a lower center frequency antenna since at X-band a 50um trace difference on a PCB already accounts for a  $1^\circ$  phase shift. A C-band antenna would be less sensitive in general and may yield more deterministic results.

To eliminate the measurement error due to the swapping of the AUT, the tests can be done by connecting a switch to the AUT. The final system proposed in section 1.3 could use a PIN diode to switch from open to short, since they offer very low series resistance in their forward biased state, while also having very high resistance in their reversed biased state.

# Bibliography

- [1] Wolff, Christian, “Feeding systems of phased arrays,” 2025. [Online]. Available: <https://www.radartutorial.eu/06.antennas/Feeding%20Systems.en.html>
- [2] Digikey, “Hmc647alp6e,” 2025. [Online]. Available: [https://www.digikey.co.za/en/products/detail/analog-devices-inc/HMC647ALP6E/5886934?gad\\_source=1&gad\\_campaignid=20282057973&gbraid=0AAAAAADrbLliXfxIdGeAvbau5GVk2\\_Z25t&gclid=Cj0KCQjwyIPDBhDBARIsAHJyyVh2D0dvsjadeNCJ\\_9vl\\_uq0K0Jmi1zNC6C50FCE0sEE4DPvopNK1eQaAhD](https://www.digikey.co.za/en/products/detail/analog-devices-inc/HMC647ALP6E/5886934?gad_source=1&gad_campaignid=20282057973&gbraid=0AAAAAADrbLliXfxIdGeAvbau5GVk2_Z25t&gclid=Cj0KCQjwyIPDBhDBARIsAHJyyVh2D0dvsjadeNCJ_9vl_uq0K0Jmi1zNC6C50FCE0sEE4DPvopNK1eQaAhD)
- [3] Kopp, Dr Carlo, “Phazotron zhuk ae/ase,” 2014. [Online]. Available: <https://www.ausairpower.net/APA-Zhuk-AE-Analysis.html>
- [4] Arar, Dr. Steve, “Transmission line theory: Observing the reflection coefficient and standing wave,” 2023. [Online]. Available: <https://www.allaboutcircuits.com/technical-articles/rf-transmission-line-theory-reflection-coefficient-and-standing-waves/>
- [5] Pozar, D. M., “Microwave engineering,” 2011. [Online]. Available: [https://www.takealot.com/microwave-engineering/PLID73727449?gad\\_campaignid=18919708446&gad\\_source=1&gbraid=0AAAAADuiBEz-RM0v1B6Rj24-D220LUrRS&gclid=Cj0KCQjw4qHEBhCDARIsALYKFNNgLGDgz0dDWVz7qCdULGDQwa-kAb-kpabDiEW-ZumsjZ\\_COKx4VzEaAge3EALw\\_wcB&gclsrc=aw.ds&gclsrc=aw.ds](https://www.takealot.com/microwave-engineering/PLID73727449?gad_campaignid=18919708446&gad_source=1&gbraid=0AAAAADuiBEz-RM0v1B6Rj24-D220LUrRS&gclid=Cj0KCQjw4qHEBhCDARIsALYKFNNgLGDgz0dDWVz7qCdULGDQwa-kAb-kpabDiEW-ZumsjZ_COKx4VzEaAge3EALw_wcB&gclsrc=aw.ds&gclsrc=aw.ds)
- [6] antenna-theory.com, “Microstrip (patch) antennas,” 2021. [Online]. Available: <https://www.antenna-theory.com/antennas/patches/antenna.php>
- [7] Stutzman, Warren L., “Antenna theory,” 2013. [Online]. Available: [https://www.takealot.com/antenna-theory-analysis-and-design/PLID41376779?gad\\_campaignid=18919708446&gad\\_source=1&gbraid=0AAAAADuiBEz-RM0v1B6Rj24-D220LUrRS&gclid=Cj0KCQjw4qHEBhCDARIsALYKFNOw906DjPInB2ZG-0DS3G1vY4986lhhsD66ouaIAa8OIKN\\_dVsdfy8aArvfEALw\\_wcB&gclsrc=aw.ds&gclsrc=aw.ds](https://www.takealot.com/antenna-theory-analysis-and-design/PLID41376779?gad_campaignid=18919708446&gad_source=1&gbraid=0AAAAADuiBEz-RM0v1B6Rj24-D220LUrRS&gclid=Cj0KCQjw4qHEBhCDARIsALYKFNOw906DjPInB2ZG-0DS3G1vY4986lhhsD66ouaIAa8OIKN_dVsdfy8aArvfEALw_wcB&gclsrc=aw.ds&gclsrc=aw.ds)
- [8] ——, “Antenna theory,” 2013. [Online]. Available: [https://www.takealot.com/antenna-theory-analysis-and-design/PLID41376779?gad\\_campaignid=18919708446&gad\\_source=1&gbraid=0AAAAADuiBEz-RM0v1B6Rj24-D220LUrRS&gclid=Cj0KCQjw4qHEBhCDARIsALYKFNOw906DjPInB2ZG-0DS3G1vY4986lhhsD66ouaIAa8OIKN\\_dVsdfy8aArvfEALw\\_wcB&gclsrc=aw.ds&gclsrc=aw.ds](https://www.takealot.com/antenna-theory-analysis-and-design/PLID41376779?gad_campaignid=18919708446&gad_source=1&gbraid=0AAAAADuiBEz-RM0v1B6Rj24-D220LUrRS&gclid=Cj0KCQjw4qHEBhCDARIsALYKFNOw906DjPInB2ZG-0DS3G1vY4986lhhsD66ouaIAa8OIKN_dVsdfy8aArvfEALw_wcB&gclsrc=aw.ds&gclsrc=aw.ds)
- [9] Circuits, All About, “The 50  $\omega$  question: Impedance matching in rf design,” 2025. [Online]. Available: <https://www.allaboutcircuits.com/textbook/radio-frequency-analysis-design/real-life-rf-signals/the-50-question-impedance-matching-in-rf-design/>

- [10] Analysis, Cadence System, “Common pcb dielectric materials and their properties,” 2025. [Online]. Available: <https://resources.system-analysis.cadence.com/blog/msa2021-common-pcb-dielectric-materials-and-their-properties>
- [11] Circuits, All About, “Wavelength (tem) calculator,” 2025. [Online]. Available: <https://www.allaboutcircuits.com/tools/wavelength-tem-calculator/>
- [12] Systems, Hawk Measurement, “What is the difference between frequencymodulated,” 2020. [Online]. Available: [https://www.hawkmeasurement.com/assets/files/FMCW\\_vs\\_Pulse\\_Radar\\_White\\_Paper\\_1.pdf](https://www.hawkmeasurement.com/assets/files/FMCW_vs_Pulse_Radar_White_Paper_1.pdf)
- [13] Merriam-Webster, “Permittivity,” 2022. [Online]. Available: <https://www.merriam-webster.com/dictionary/permittivity>
- [14] ——, “Permeability,” 2022. [Online]. Available: <https://www.merriam-webster.com/%20dictionary/permeability>
- [15] microwaves101, “S-parameters,” 2022. [Online]. Available: <https://www.microwaves101.com/encyclopedia/s-parameters>
- [16] Coonrod, John, “Understanding when to use fr-4 laminates or high frequency laminates,” 2010. [Online]. Available: [https://www.electronics.org/system/files/technical\\_resource/E6%26S21\\_03.pdf](https://www.electronics.org/system/files/technical_resource/E6%26S21_03.pdf)

# Appendix A

## Repository Locations

All code designed for this project can be found at the following link:

[https://github.com/bcj2307/Phase-encoding-a-reflector-array-using-open-and-short-circuited-loads/  
tree/main/MATLAB](https://github.com/bcj2307/Phase-encoding-a-reflector-array-using-open-and-short-circuited-loads/tree/main/MATLAB)

All CST simulation used for the antenna design for this project can be found at the following link:

[https://github.com/bcj2307/Phase-encoding-a-reflector-array-using-open-and-short-circuited-loads/  
tree/main/CST](https://github.com/bcj2307/Phase-encoding-a-reflector-array-using-open-and-short-circuited-loads/tree/main/CST)

All Altium files used for the manufacturing of the antenna can be found at the following link:

[https://github.com/bcj2307/Phase-encoding-a-reflector-array-using-open-and-short-circuited-loads/  
tree/main/Altium](https://github.com/bcj2307/Phase-encoding-a-reflector-array-using-open-and-short-circuited-loads/tree/main/Altium)

Furthermore, the L<sup>A</sup>T<sub>E</sub>X source code for this report, as well as the SVG and PDF diagrams that were designed and included, can be found at:

[https://github.com/bcj2307/Phase-encoding-a-reflector-array-using-open-and-short-circuited-loads/  
tree/main/Report](https://github.com/bcj2307/Phase-encoding-a-reflector-array-using-open-and-short-circuited-loads/tree/main/Report)